thermal or may be due to a slow trend of the Digicon electric fields toward equilibrium. Figure 7.1-16 shows an optical bench temperature over the time period that the aperture repeatability data was taken. The drift of five to six microns from time 100 to 300 minutes with a temperature change of about one degree is consistent with the thermal motion measured on the blue side over a 5-degree temperature transition. Over the 5 degrees, the blue side showed an average of 6.4 microns per degree shift (see Figure 7.1-17). Figures 7.1-11 to 7.1-15 also show that the aperture wheel is repeatable to within a micron (as measured by the scatter of the data points from a smooth line).

7.2 Aperture and Filter-Grating Wheel Repeatability

7.2.1 Initial Instrument-Level Tests

Repeatability of the grating wheel was measured by locating the position of the 0.1 arcsec aperture in an aperture map after the grating wheel had been moved to various positions. Shifts of up to 10 microns in both X and Y detector coordinates were detected. To check for repeatability over longer time intervals, additional measurements were derived from other ambient calibrations. A shift of -0.45 $\pm$ .02 diode (23 $\pm$ 1 micron) in X on the detector occurred between two H57 A4 spectra made 7 hrs apart. Furthermore, aperture maps made on different dates are shifted up to 0.28 diode (14 microns) in X. The shifts in spectral position that are associated with rotation of the filter-grating wheel are pushing the limits of acceptability for good photometric repro-

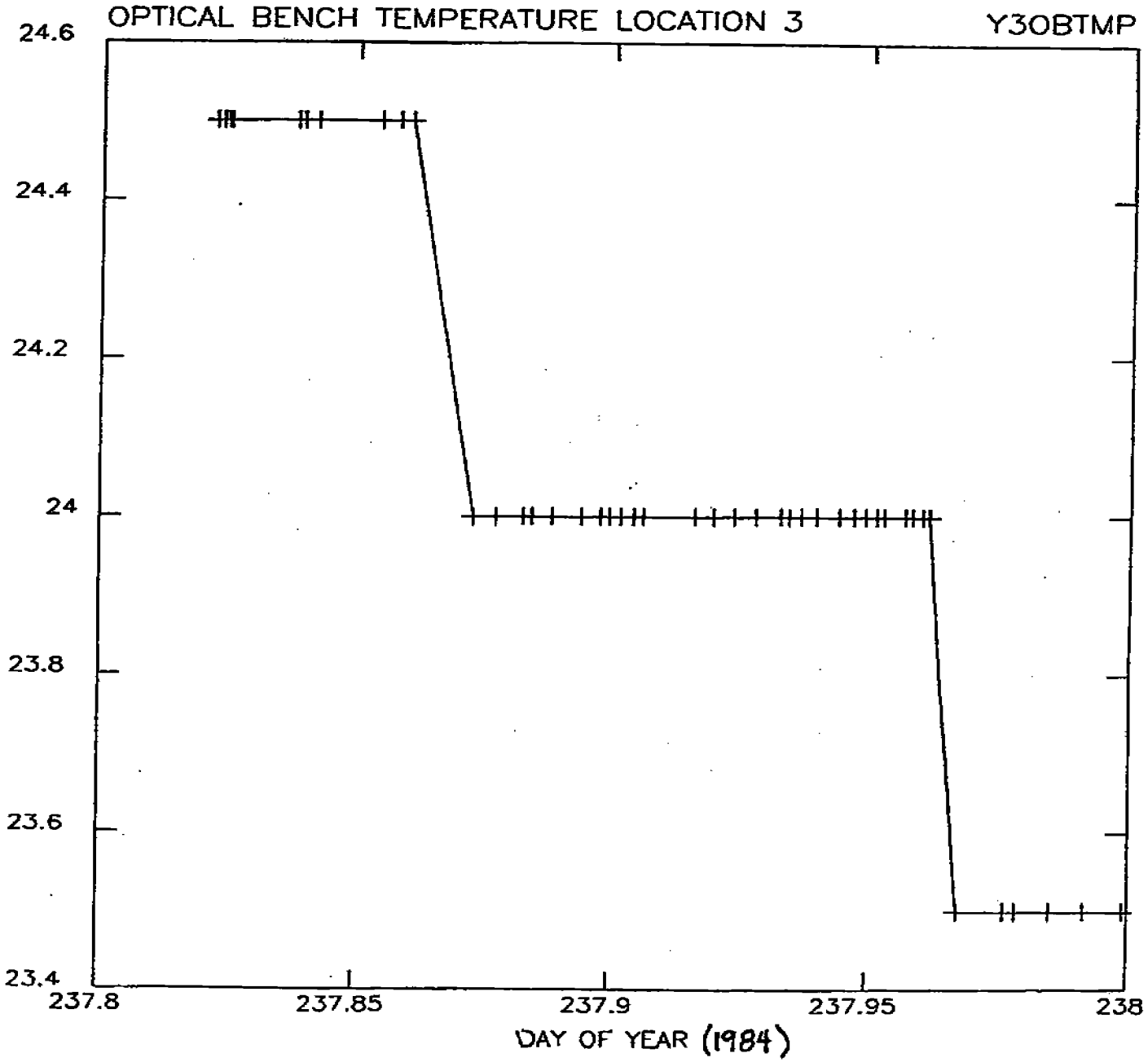
OPTICAL BENCH TEMPERATURE LOCATION 3
Y3OBTMP
24.6
24.4
24.2
24
23.8
23.6
23.4
DEGREES (C)
237.8
237.85
237.9
237.95
238
DAY OF YEAR (1984)

FIGURE 7.1-16

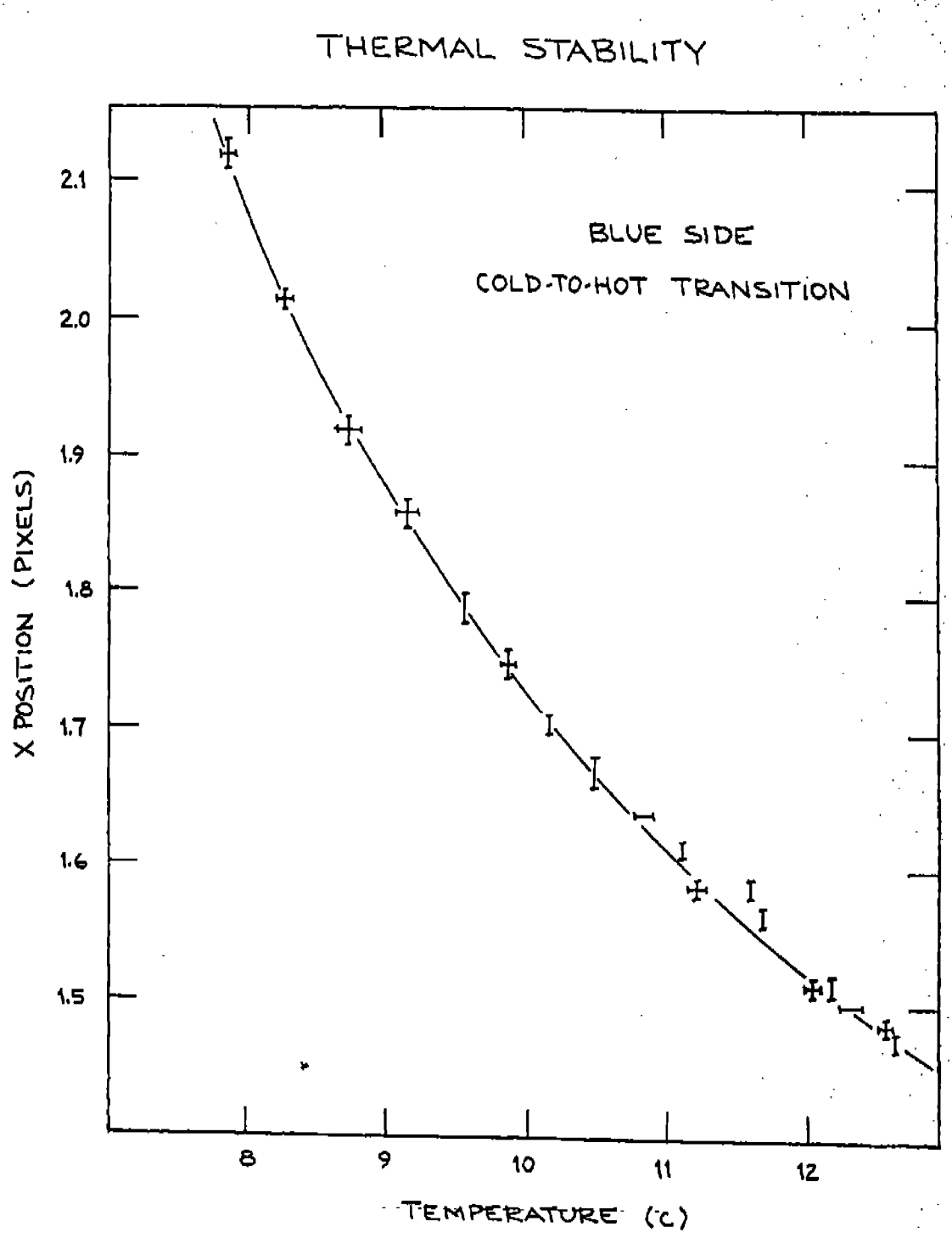

FIGURE 7.1-17
-297-

ducibility. The detent mechanism of the filter-grating wheel and the seating of the camera mirror should be checked.

A series of external Pt-Cr-Ne emission line spectra were made with different apertures in the ambient calibration of March, 1983 to determine how well the position of the aperture wheel repeated. The nine spectra, made with grating H57 and eight x-steps, were taken with the red detector over a 75-minute interval in the following order:

1	2	3	4	5	6	7	8	9
C2	C2	C2	B2	A4	B2	C2	B2	A4

To determine whether there are systematic shifts between spectra, a cross-correlation technique is used. The spectra are correlated in 100 diode bins. As there are no spectral lines in the last bin (diodes 400-500), only the results of the first four bins are considered. In each comparison, there are no systematic shifts as a function of bin number, an indication that the spectra are linearly translated, but not stretched. In Table 7.2.1-1, the average of the first four bins is presented as a measure of the shift between spectra.

With the exception of a .014 $\pm$ .002 diode shift between trials 3 and 7 with aperture C2, the spectra repeated to .004 of the diode separation or better, which is the accuracy of the measurements. The diode separation is 50 microns in the X-direction. From these motions on the diode array, we can calculate the corresponding tangential motion of the aperture wheel from the geometry. The dispersion direction is angled approximately

Table 7.2.1-1

APERTURE REPEATABILITY MEASURED BY CROSS-CORRELATION OF SPECTRA

Aperture	Trials	Shift on Detector (Diodes)	Shift on Aperture Wheel (Microns)
C2	1,2	.002 +/- .001	0.4 +/- 0.2
C2	1,3	.002 +/- .003	0.3 +/- 0.5
C2	1,7	.014 +/- .002	2.3 +/- 0.3
B2	4,6	.004 +/- .002	0.6 +/- 0.3
B2	6,8	-.002 +/- .005	-0.3 +/- 0.2
A4	5,9	-.001 +/- .005	-0.2 +/- 0.8
Offsets Between Apertures, for Comparison:			
C2,A4	1,9	.177 +/- .011	30.1 +/- 1.9
B2,A4	4,9	.059 +/- .006	10.0 +/- 1.0

54 degrees to the tangent of the aperture wheel. This, combined with the 2X difference in scale between the detector and the aperture wheel, determines the relation between motion on the detector (d) and motion of the aperture wheel (x):

$$x = \frac{2d}{\cos(54^{\circ})} \approx 3.4d$$

Applying this to the measured shifts, we find that the aperture wheel shifted 2.3 ± 0.3 microns between trials 3 and 7 with C2, compared with 0.6 microns or less for the other trials. The large shift occurred when the wheel was cycled through B2, A4 and B2 before returning to C2.

The repeatability of the grating wheel was measured in March 1983 by projecting an image of the 0.1 arcsec paired aperture onto the photocathode with the camera mirror. In between these aperture maps, the grating wheel was rotated to other grating positions and then returned to the camera mirror. Ten aperture maps were made in a 90-minute interval in the following order.

map1 PRI map2 H57 map3 H19 map4 H40 map5 H78
map6 H27 map7 H40 map8 H13 map9 L15 map10

Using the red detector, 68 y-steps of 11.29 microns each were made with a 20-diode wide section of the diode array (diodes 254-273), which was quarter-stepped and overscanned by 5 diodes. This produces a 96 x 68 aperture map with an effective sampling size of 12.5 microns in X and 11.3 microns in Y. Because the true 14 x 14 micron aperture image is convolved with the

50 x 200 micron FOS diode area, the aperture map produces an image approximately the same size as a diode.

The center of an aperture image is measured by first computing the average cross-section of the aperture (sum of the counts) in each dimension. A centroid of this cross-section is used to compute the center of the aperture. For example, in the X-direction, the center of the aperture is given by:

$$\overline{X} = \frac{\sum X * C}{\sum C},$$

where x is the X-coordinate and C is the number of counts in each x-step. The expression for Y is the same but with y-steps substituted for x-steps. The conversion between y-steps and y-position on the detector is: y-position (microns) = y-base + 11.23 microns * y-steps. The y-base used for these aperture maps is -393 microns.

The positions of the upper and lower halves of the paired aperture are shown in Table 7.2.1-2. The motion of the upper aperture corresponds to that of the lower to within 0.07 diode (3.5 microns) in X, and 0.13 y-steps (1.5 micron) in Y, suggesting that the measurement of the aperture positions is at best this accurate. Visual examination of the aperture maps clearly shows the shifts. An example is the contour plot in Figure 7.2.1-1 where trial 7 (dashed line) is compared with trial 8 (solid line).

In the Y-direction, an increase of 7 microns occurred between trials 1 and 2, followed by a slow decline of 10 microns between trials 2 and 8. The x-position repeats to better than

Table 7.2.1-2

FGW REPEATABILITY: CENTROIDED POSITIONS OF 0.1 ARCSEC APERTURE IMAGES

Grating		X-Position (Diodes) L	X-Position (Diodes) U	Y-Position (Microns) L	Y-Position (Microns) U
1	CAM PRI	267.877	267.720	-171.3	243.9
2	CAM H57	267.861	267.663	-164.3	251.5
3	CAM H19	267.905	267.747	-166.0	250.1
4	CAM H40	267.894	267.708	-166.1	248.6
5	CAM H78	267.916	267.745	-171.3	244.6
6	CAM H27	267.914	267.742	-171.0	245.2
7	CAM H40	267.928	267.772	-172.1	243.2
8	CAM H13	267.130	267.991	-173.5	243.1
9	CAM L15	268.098	267.892	-168.5	246.8
10	CAM	268.076	267.924	-171.6	243.9

L = LOWER

U = UPPER

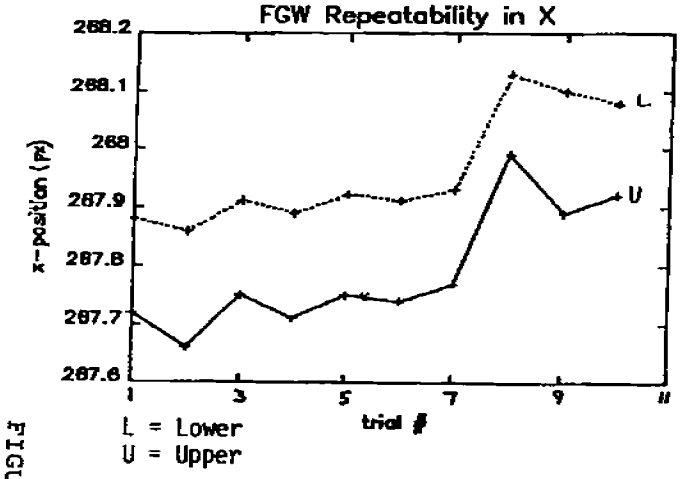
FGW Repeatability in X
x-position (M)
trial #
L
U
L = Lower
U = Upper

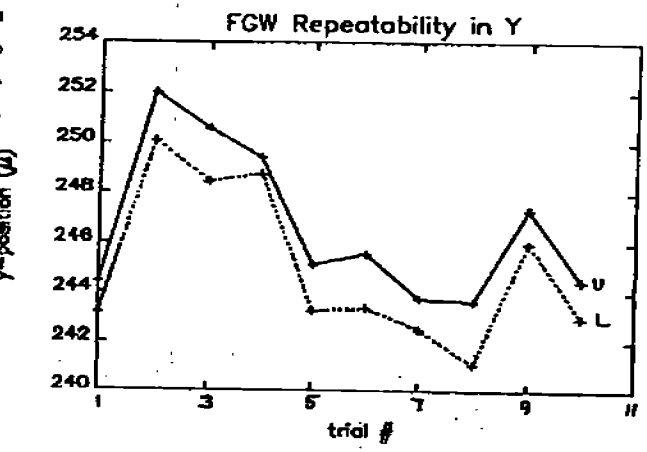
FGW Repeatability in Y
y-position (M)
trial #
U
L

FIGURE 7.2.1-1

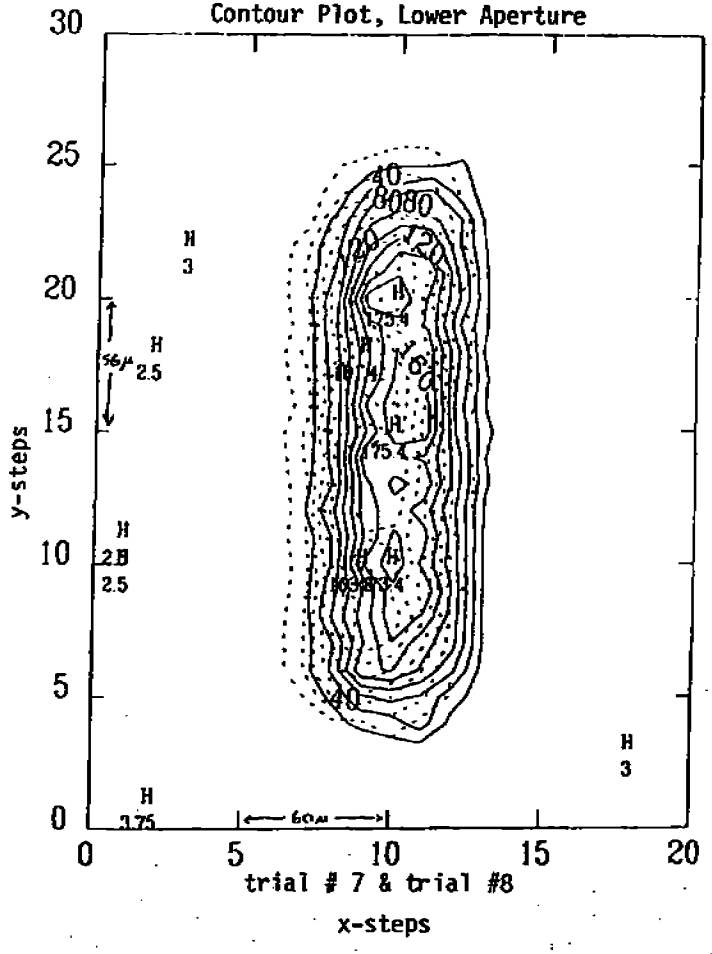
Contour Plot, Lower Aperture
y-steps
x-steps
trial # 7 & trial #8
60μ
56μ

0.1 diode (5 microns) in trials 1-7, but both apertures shift 0.2 diode (10 microns) between trials 7 and 8. The wheel was moved to grating H40 between these trials, as was the case between trials 4 and 5, but no anomalous shift occurred there. The dispersion direction is oriented radially on the grating wheel, so that rotation of the wheel produces a movement in the Y direction on the detector.

Additional spectra taken in the internal-external offset and internal wavelength calibrations show much larger changes in the x-position of spectra from day to day in the March 1983 calibration. The external H57 A4 red spectrum obtained seven hours after the repeatability data is shifted -0.45 $\pm$ .02 diode (23 $\pm$ 1 microns) from trial 1 of the repeatability calibration, compared with internal-external offsets ranging from 0.01 to 0.07 diode (0.5 to 3.5 microns). The H57 internal wavelength spectrum obtained 40 hours earlier is shifted only -.04 $\pm$ .02 diode (-2 $\pm$ 1 microns) from trial 1. Furthermore, the A4 map for part 10B of the aperture map calibration, which was made 13 hours before the FGW repeatability maps, is shifted 0.28 diode (14 microns) in X, but less than 0.5 micron in Y.

The FOS notebook and the tape log indicate that the detector was used prior to these calibrations, so that it is unlikely that power-up settling times caused the shifts. In the ambient calibration, the temperature should have remained roughly constant, so that thermal shifts should not be a factor. No standard header packets were obtained with the March data, so that correlation of the shifts with temperature cannot be checked. One

theory to explain the observations is that the camera mirror might be loose in its fixture. Another possibility is that we are seeing slop in the filter-grating wheel detents, which could be uncorrelated in X and Y. Results are summarized in Tables 7.2.1-1 and 7.2.1-2.

7.2.2 Improvements in Filter-Grating Wheel Repeatability

The filter-grating wheel repeatability can be significantly improved by applying an additional motor step after the initial, standard positioning of the wheel. Both the standard deviation and spread in the positions of spectral images along the dispersion axis were reduced by a factor 2 with the extra step applied. However, the degree to which this remedy will alleviate the repeatability problem in actual flight conditions, especially for the camera mirror, is uncertain. Because the residual non-repeatability will most likely remain unsatisfactory and thermal variations will also cause significant image drift, modifications to the FOS to permit direct image location (addition of aperture-illuminating LEDs) was undertaken late in 1985.

An attempt has also been made to improve the FGWA repeatability by applying a small offset force to the wheel after it has been nominally positioned at the desired disperser (or camera mirror) and then allowing it to relax into that position. This was accomplished by commanding one additional step of the FGWA stepper motor in the forward direction after performing standard positioning (also in the forward direction). Power to the motor is removed immediately after the motor is phased for this step for the usual (200 ms) duration, allowing the detent

roller to perform the final positioning adjustment from a more repeatable initial condition than is likely without this extra step.

Preliminary tests were conducted on February 20, 1985 during which the image position (in the dispersion (x) direction only) of a line near the center of the H40 grating (red side) spectrum of the internal calibration lamp was measured. Spectra were taken after normal positioning of the FGWA and after application of the additional motor step. Thirteen trials were made, with the FGW rotated 360 degrees between each trial. It was readily apparent that the repeatability could be improved with this process; in every case for which the wheel initially settled to a position with large deviation from the mean, application of the extra step reduced the discrepancy markedly. The standard deviation in the spectral line image position was reduced from about 9 microns (before motor step) to just over 5 microns afterwards. Tests with one step in each direction applied consecutively appeared to make no additional improvement. Trials were also made with 2 additional forward steps applied, which sometimes drove the wheel far enough that the detent roller moved entirely out of the detent, so that the positioning was lost.

In order to test the effectiveness of this method further, for other FGW positions, the standard repeatability test procedure was performed on March 6, 1985, on the blue side. The results of this test can be directly compared to those of the October 16, 1984 evaluation, which yielded a mean standard deviation of 6.9 microns in the X direction for 9 trials of each

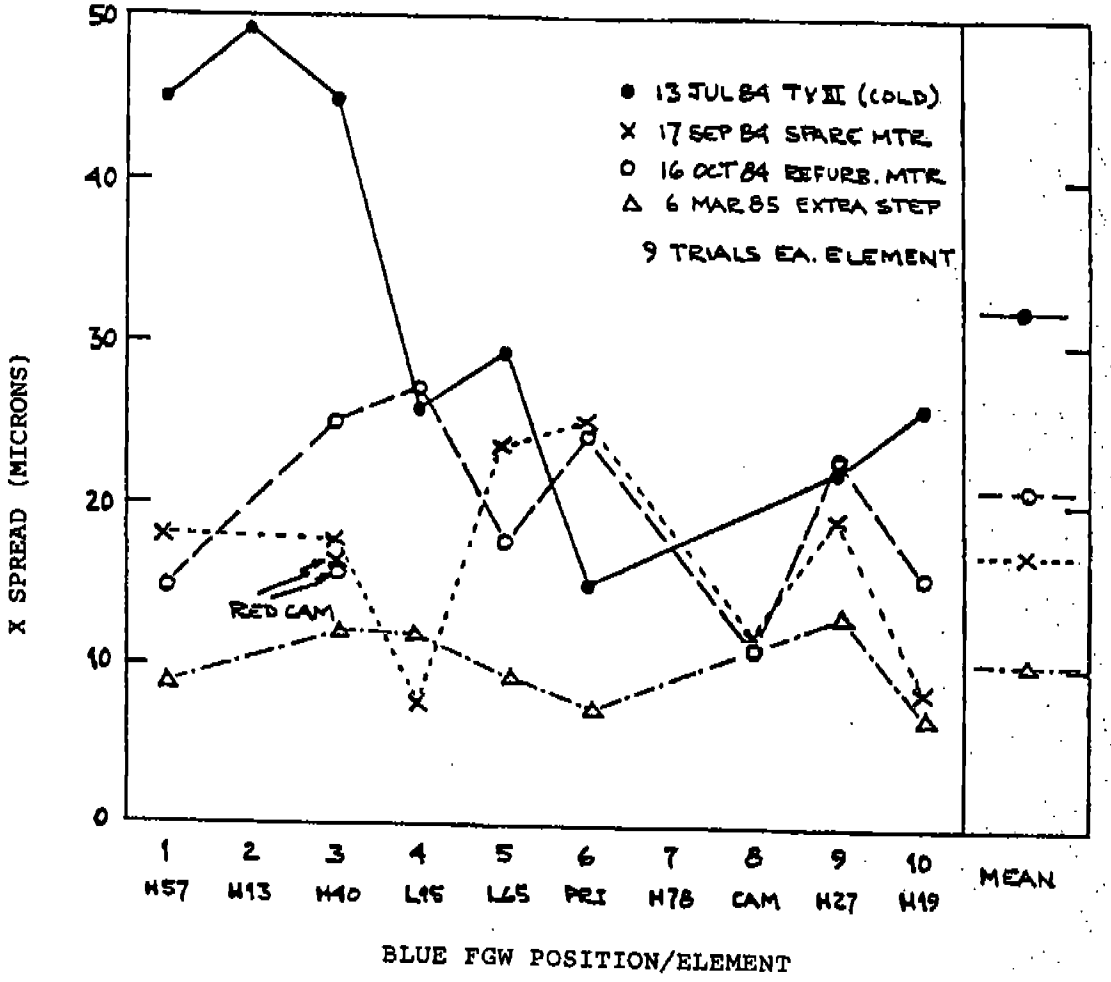
50
40
30
20
10
0
X SPREAD (MICRONS)
13 JUL 84 TYII (COLD)
17 SEP 84 SPARE MTR.
16 OCT 84 REFURB. MTR.
6 MAR 85 EXTRA STEP
9 TRIALS EA. ELEMENT
RED CAM
1 H57
2 H13
3 H40
4 L46
5 L65
6 PRI
7 H78
8 CAM
9 H27
10 H19
MEAN
BLUE FGW POSITION/ELEMENT

FIGURE 7.2.2-1

previous FGWA repeatability test data. An additional concern is that these measurements were made in ambient, whereas the previous data indicate that the repeatability may be significantly worse when the FGW is operated under colder flight conditions.

We conclude that, if possible, a direct evaluation of the FGWA repeatability for the camera mirror, on both red and blue sides and in both X and Y axes, should be made during thermal-vacuum testing. Furthermore, the addition of a means of illuminating the entrance apertures (LEDs) and the minor modifications to the NSSC-1 software required to determine the aperture image positions will significantly aid our ability to perform accurate target acquisitions, whether or not the improvements to the FGWA repeatability suggested by our recent tests will indeed be realized on orbit. The LEDs were installed into the FOS during December, 1985.

8.0 SPECTROPOLARIMETER

The Faint Object Spectrograph of the Space Telescope will be able to obtain spectropolarimetric data on faint astronomical objects. This is done by introducing a Wollaston prism and rotating waveplate behind the spectrograph entrance apertures. Tests of the polarimeter and its optics have demonstrated that the device is capable of excellent performance. The magnesium fluoride optical components of the polarimeter permit measurements of linear and circular polarization throughout the ultraviolet, down to Lyman α at 1216 Å. The mechanical stability and repeatability of the mechanism are demonstrated to yield position angles of the incoming plane of polarization to better than $\pm$ 0.5 degree, and we anticipate that measurements of the degree of polarization could be made to an accuracy of at least 0.1%. The accuracy for faint objects will depend on the integration times available for the observations, because of noise from photoelectron statistics. A 20-minute integration at 15th magnitude gives typically errors of 1% in each 100 Å wide spectral band.

8.1 Basic Principles

The polarization of a source can be characterized by the four Stoke's parameters I_1, Q_1, U_1, V_1 in the coordinate system shown in Figure 8.1-1. The degree of linear polarization in such a system is

$$P = \frac{(Q_1^2 + U_1^2)^{\frac{1}{2}}}{I_1}, \qquad (8.1\text{-}1)$$

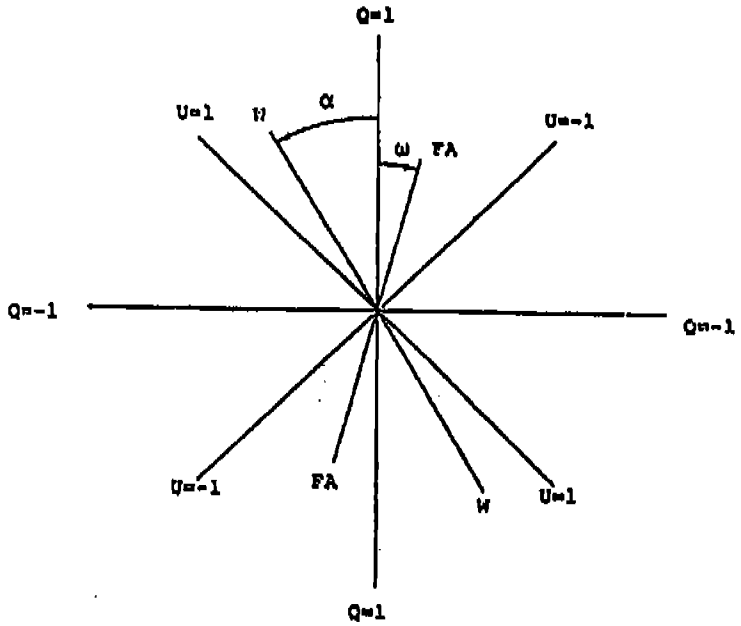

Figure 8.1-1. Coordinate system used in the polarization analysis. The view is toward the source. The line W-W is the pass direction of the Wollaston; while FA-FA is the fast axis of the waveplate.

the position angle of the plane of polarization is

$$\theta = 1/2 \tan^{-1}\left(\frac{U_1}{Q_1}\right),$$

the degree of circular polarization is

$$P_V = \frac{V_1}{I_1}, \tag{8.1-2}$$

and the intensity is

$$I_1 = I_0 + (Q_1^2 + U_1^2 + V_1^2)^{1/2} \tag{8.1-3}$$

where I_0 is the unpolarized component of I_1.

If a waveplate with a fast axis at an angle ω and a retardation δ is inserted between the source and an observer, the transmitted radiation will have a new polarization state

$$I_2 = I_1. \tag{8.1-4}$$

$$Q_2 = (1/2(1 + \cos\delta) + 1/2(1 - \cos\delta)\cos 4\omega)Q_1 - (1/2(1 - \cos\delta)\sin 4\omega)U_1 + (\sin\delta \sin 2\omega)V_1. \tag{8.1-5}$$

$$U_2 = -(1/2(1 - \cos\delta)\sin 4\omega)Q_1 + (1/2(1 + \cos\delta) - 1/2(1 - \cos\delta)\cos 4\omega)U_1 + (\sin\delta \cos 2\omega)V_1. \tag{8.1-6}$$

and

$$V_2 = -(\sin\delta \sin 2\omega)Q_1 - (\sin\delta \cos 2\omega)U_1 + (\cos\delta)V_1. \tag{8.1-7}$$

If the observer then places an analyzer at an angle α in back of the waveplate, he will detect a signal

$$J = 1/2(I_2 + Q_2\cos 2\alpha + U_2\sin 2\alpha). \qquad (8.1\text{-}8)$$

In cases where the analyzer and coordinate system are aligned so that $\alpha = 0$, the observer receives a signal

$$J = \frac{I_1}{2} + \frac{Q_1}{4}(1 + \cos\delta) + \frac{Q_1}{4}(1 - \cos\delta)\cos 4\omega - \frac{U_1}{4}(1 - \cos\delta)\sin 4\omega + \frac{V_1}{2}\sin\delta \sin 2\omega. \qquad (8.1\text{-}9)$$

By defining a phase factor $\epsilon = 2\theta + 90^{\circ}$ such that

$$\sin\epsilon = \frac{Q_1}{(Q_1^2 + U_1^2)^{\frac{1}{2}}} = +\cos 2\theta \qquad (8.1\text{-}10)$$

and

$$\cos\epsilon = \frac{-U_1}{(Q_1^2 + U_1^2)^{\frac{1}{2}}} = -\sin 2\theta, \qquad (8.1\text{-}11)$$

this expression can be reduced to

$$J = \frac{I_1}{2} + \frac{Q_1}{4}(1 + \cos\delta) + \frac{(Q_1^2 + U_1^2)^{\frac{1}{2}}}{4}(1 - \cos\delta)\sin(4\omega + \epsilon) + \frac{V_1}{2}\sin\delta \sin 2\omega. \qquad (8.1\text{-}12)$$

The functional dependence of J on ω in this equation shows that a rotating waveplate in front of an analyzer will modulate a linearly polarized beam at 4 times its rotation rate; while a circularly polarized beam will be modulated at 2 times its rotation rate. This equation also shows that, if one can determine the waveplate retardation δ, measures of J as a function of ω can

be used to determine the Stoke's parameters I_1, Q_1, U_1, V_1 of the source.

The retardation of the rotating waveplate can be determined experimentally with 100% linearly polarized light. Under such conditions, $I_1 = (Q_1^2 + U_1^2)^{1/2}$ and

$$\delta = 2 \cos^{-1} \left(\frac{1 - M}{1 + M \sin \epsilon}\right)^{\frac{1}{2}} \qquad (8.1\text{-}13)$$

where $M = \frac{J_{max} - J_{min}}{J_{max} + J_{min}}$ is the observed modulation of the signal. If the plane of polarization of the incoming radiation is aligned with the pass direction of the Wollaston prism, then $\sin \epsilon = 1$ and

$$\delta = 2 \cos^{-1} \left(\frac{J_{min}}{J_{max}}\right)^{\frac{1}{2}}. \qquad (8.1\text{-}14)$$

This is the best configuration for measuring δ. When the incoming plane of polarization is more nearly perpendicular to the Wollaston prism pass direction, δ is very uncertain because $1 - M$ and $1 + M \sin\epsilon$ are both very small.

8.2 The Polarimeter Mechanism

The FOS polarimeter contains two rotatable waveplate retarders and two Wollaston prisms. One waveplate is permanently located in front of each Wollaston. The polarimeter is designed so that only a single motor is required to rotate the waveplates and to move either of the Wollaston/waveplate pairs from one entrance port to the other or out of the way. The mechanism that

accomplishes this is shown in Figure 8.2-1. The drum, which is only 1.9 inches in diameter, contains the two Wollaston/waveplate pairs. The Wollastons are permanently fixed to the drum, but the waveplates are mounted in rotatable cylinders inside the drum. The waveplate cylinders have a 16-tooth gear on the outside which meshes with a 17-tooth fixed center gear inside the drum. One revolution of the drum rotates the Wollastons by 360°. The waveplates, however, rotate 382.5°. Each rotation of the drum thus increments the position angle of the waveplate fast axis by a net 22.5°. Sixteen rotations of the drum bring the mechanism back to its original configuration.

The drum is driven by a 90° permanent magnet stepper motor. A total of 420 motor steps are required to rotate the drum 360°. Errors in the positions of the optical components result from tolerances on the motor (± 4.5°) and from errors in the gear train. Anti-backlash gears have been used wherever possible, and clearances between bearings and their housings and shafts have been held to less than .0001". Each bearing is also preloaded axially to eliminate radial play within the bearing itself. Belleville washers and compression springs provide the necessary preloads. Repeatability tolerances on θ_z (rotation about the optical axis) are ± 2.8 arc min for the Wollaston prisms and ± 10.0 arc min for the waveplates. Tolerances on θ_x and θ_y are ± 1.7 arc min for the Wollaston prisms and ± 3.0 arc min for the waveplates. These mechanical tolerances are better than those originally specified for the mechanism and will help to minimize

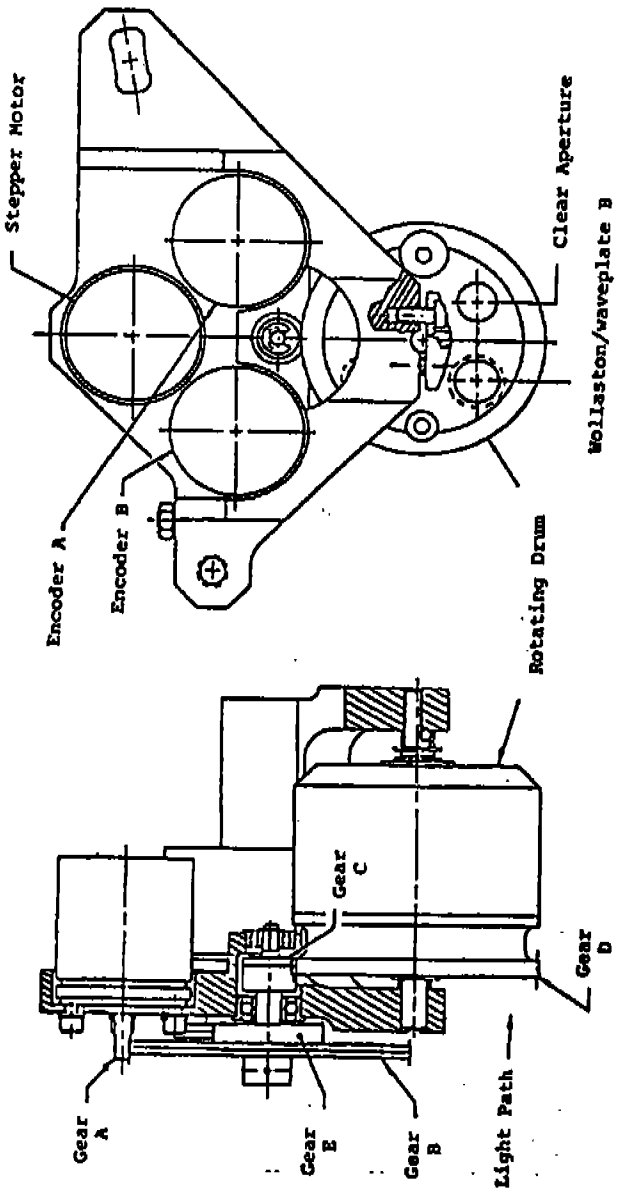

Figure 8.2-1. Side and rear views of the polarimeter.

uncertainties in the measurements that might be introduced by errors in the positions of the components.

Figure 8.2-2 shows the relative positions of the two Wollaston/waveplate pairs, labeled A and B, and the clear apertures, labeled C. The clear apertures are located in the red and blue beams. Motor step counts and angles between the various elements are indicated.

Two eight-bit pin encoders provide positional information on the mechanism. One revolution of the drum rotates encoder A five times and encoder B 5.0625 times. In 16 cycles, encoder A rotates 80 times and encoder B 81 times, bringing both back to their original counts. Encoder A changes by 3.0476 bits and encoder B by 3.0857 bits with each step of the motor. Both encoders increase with a CCW rotation of the drum as viewed in Figure 8.2-2. If the motor should ever fail, the entire mechanism can be removed from the optical path by activating a hot wire pinpuller.

8.3 Subassembly-Level Performance

The Wollaston prisms and waveplates for the polarimeter were manufactured by the Karl Lambrecht Corp. of Chicago, Illinois. Magnesium fluoride was the birefringent crystal selected for the polarizing elements because of its transmission to below 1200 Å. The birefringence of magnesium fluoride changes slowly in the visible and near UV. Around 1200 Å, however, it falls to zero and then has a reversed sign down to the transmission cutoff of the crystal. The Wollaston prisms both have an internal wedge

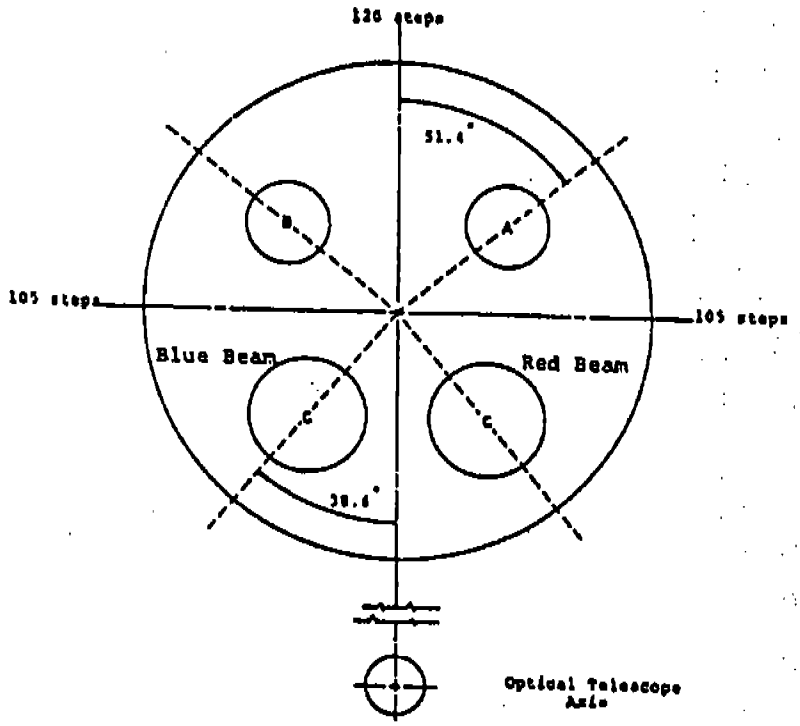

Figure 8.2-2. Relative configuration of the optical elements as viewed from inside the FOS in the direction of the entrance ports.

angle of 20°. This angle was chosen so that the weak birefringence at Lyman α would still give adequate separation for the spectra at the detector. Two waveplates with different retardations are used in the polarimeter. The thickness differential of waveplate A is 137 μm; that for waveplate B is 68.6 μm. The actual retardations and transmissions of the flight waveplates were measured as a function of wavelength at the Marshall Space Flight Center in Huntsville, Alabama. The retardations of the two flight waveplates are listed in Table 8.3-1. The wavelength of zero retardation is slightly different for the two, which we believe must be due to slightly different chemical compositions. Retardations in the FUV are presented graphically in Figure 8.3-1.

The modulation efficiency of a waveplate is equal to $1/2(1 - \cos\delta)$ for linearly polarized light and $\sin\delta$ for circularly polarized light (see Equation 8.1-12). Each waveplate is therefore most efficient at modulating linearly polarized light when $\delta = 180°$ and least efficient when $\delta = 0°$ or 360°. For circular polarization, the efficiency peaks at $\delta = 90°$ and 270°. The modulation efficiency of each waveplate as a function of wavelength has been included in Table 8.3-1. In particular, note that waveplate A has a high modulation efficiency for linear polarization at Lyman α; while waveplate B does not. Together, the two waveplates provide adequate coverage of the spectrum.

A transmission curve for the complete polarizer is shown in Figure 8.3-2. Only a single curve is shown, since both Wollaston/waveplate pairs are very similar. The fairly high

TABLE 8.3-1

RETARDATIONS OF THE FLIGHT WAVEPLATES

λ(Å)	Waveplate A			Waveplate B		
	δ	Efficiency linear	Efficiency circular	δ	Efficiency linear	Efficiency circular
1175	-108°	.65	.95	-93°	.53	1.00
1200	100°	.59	.98	0°	0	0
1216	215°	.91	.57	90°	.50	1.00
1250	360°	0	0	161°	.97	.33
1300	460°	.59	.98	228°	.83	.74
1350	482°	.76	.85	247°	.70	.92
1400	485°	.79	.82	250°	.67	.94
1450	480°	.75	.87	241°	.74	.87
1500	468°	.65	.95	238°	.76	.85
1600	439°	.85	.98	226°	.85	.72
2537	251°	.66	.94	123°	.77	.86
3650	163°	.98	.29	84°	.45	.99
6328	95°	.54	.99	43°	.13	.68

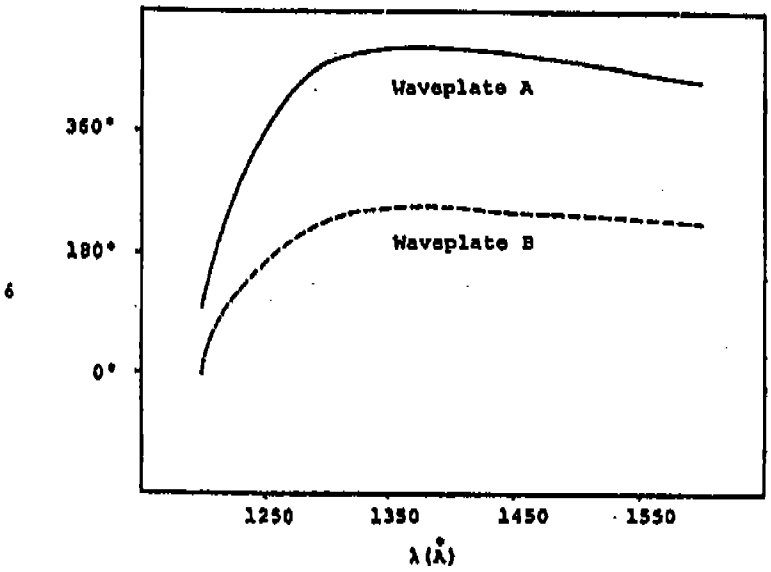

Figure 8.3-1. Retardations of the flight waveplates

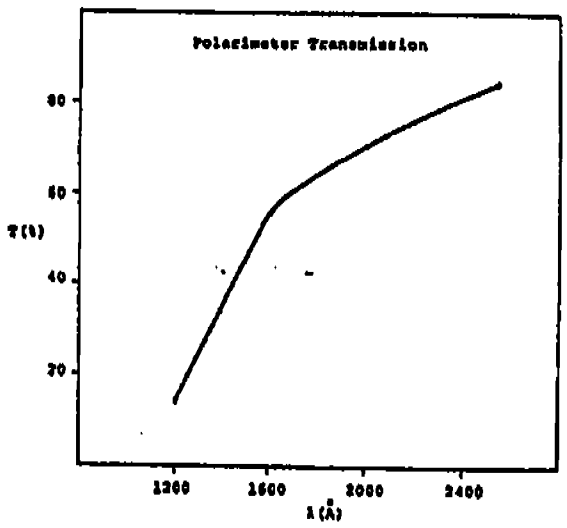

Figure 8.3-2. The transmission of the polarimeter as a function of wavelength

transmission in the FUV was achieved by carefully selecting components and by making them as thin as possible. The Wollaston prisms are 3.5 mm thick, while the waveplates are only 1.0 mm thick. All elements have an 8 mm clear aperture.

Although the manufacturer came very close to achieving the specified values of retardation for the waveplates, they were unable to optically contact them as originally desired. There is therefore some light lost at the internal boundaries of the two halves of the waveplates. The Wollaston prisms are also not optically contacted. Optically contacting the optical components would probably have been possible if the components had been scaled up in thickness. This is a tradeoff, however, that would have significantly increased the absorption losses in the FUV.

Dow Corning 6-1104 sealant was applied to the edges of the Wollastons and waveplates to hold them together during testing. The flight components were later glued into their holders in the polarimeter with the same material.

8.3.1 Laboratory Measurements

Operational tests of the polarimeter assembly were carried out at the Martin Marietta Aerospace Co. in Denver, Colorado. In the first phase of testing, the polarimeter was placed in auxiliary optical system that accurately simulated its operation in the FOS, and the position of each image in the focal plane was measured to an accuracy of $\pm$ 2.5 μm as the polarimeter was cycled from one waveplate pair, and random variations in the positions of the images were less than $\pm$ 5.0 μm. Since the digicon diodes

are 50 μm wide, there should be no significant image motion problems with the polarimeter.

The measurements of image motion were used to compute the position angles of the image splitting for the four normal configurations of the polarimeter. Figure 8.3-3 summarizes these measurements. It also shows how the images are rotated by the grazing incidence mirror and then inverted by the collimator and grating before reaching the detector. Figure 8.3-3 has a rotational orientation that is identical to that of Figure 8.2-2.

The twin images at the detector are separated by an amount

$$s = 150\ |n_e - n_o|\ \tan 20 \qquad (8.3\text{-}1)$$

where $n_e - n_o$ is the birefringence of the magnesium fluoride and s is in millimeters. Maximum splitting is 780 μm at 1530 Å. Images at Lyman α are separated by only 242 μm. Figure 8.3-3 shows that splitting is not precisely perpendicular to the dispersion. This is a consequence of requiring either waveplate to be operable in either beam.

The second phase of the operational tests involved actually measuring the polarization angle θ of a known source. In this stage of the testing, a pinhole light source at 3660 Å was placed 150 mm in front of the polarimeter. A lens after the polarimeter limited the transmitted beam to f/24 and reimaged the light onto a photomultiplier. The 2:1 imaging in the FOS was also reproduced. A chopper was used to reduce the effects of stray light. During the actual tests, an HNP'B polarizer was aligned at $\theta = 0^0$, 45^0, 90^0, and 135^0 in front of the polarimeter. At each

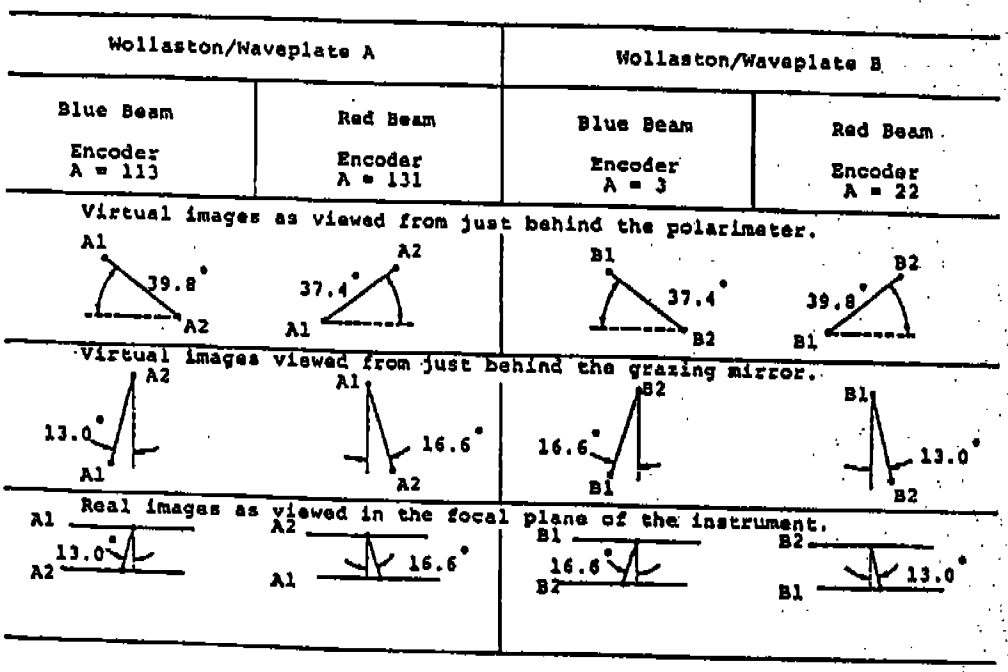

Figure 8.3-3. Split images of the entrance ports as viewed from various locations in the FOS

angle of incoming polarization, two sets of sixteen measures of the intensity J as a function of waveplate angle γ were taken with each Wollaston/waveplate pair. One set was taken with each split image. The waveplate angle changed by 22.5° between measures and was defined to be zero at the initial position of the waveplate in each data set.

The individual data sets from the tests were fitted with an equation of the form

$$J = C_1 + C_2 \sin (4\gamma + \psi). \qquad (8.3\text{-}2)$$

The phase angle ψ in this equation equals $4\omega_1 + \epsilon$, where ω_1 is the initial position of the waveplate with respect to the Wollaston pass direction and ϵ is the phase factor in Equations (8.1-10 to 8.1-12). The angle γ is thus equal to $\omega - \omega_1$ where ω_1 was determined from the eight sets of data that were taken with each Wollaston/waveplate pair. Each individual data set then yielded a final value for the angle of polarization θ and the waveplate retardation δ. Results of the test observations are summarized in Figure 8.3-4. The standard deviation of θ about its known direction is 0.15° for waveplate A and 0.22° for waveplate B. Waveplate A has a high modulation efficiency at the test wavelength; while waveplate B has a modulation efficiency of only 45%. Since these errors are consistent with known sources of error and instability in the test measurements, we can anticipate even better accuracy in the FOS.

8.3.2 Accuracy for Faint Objects

For many objects studied with the FOS polarimeter, the

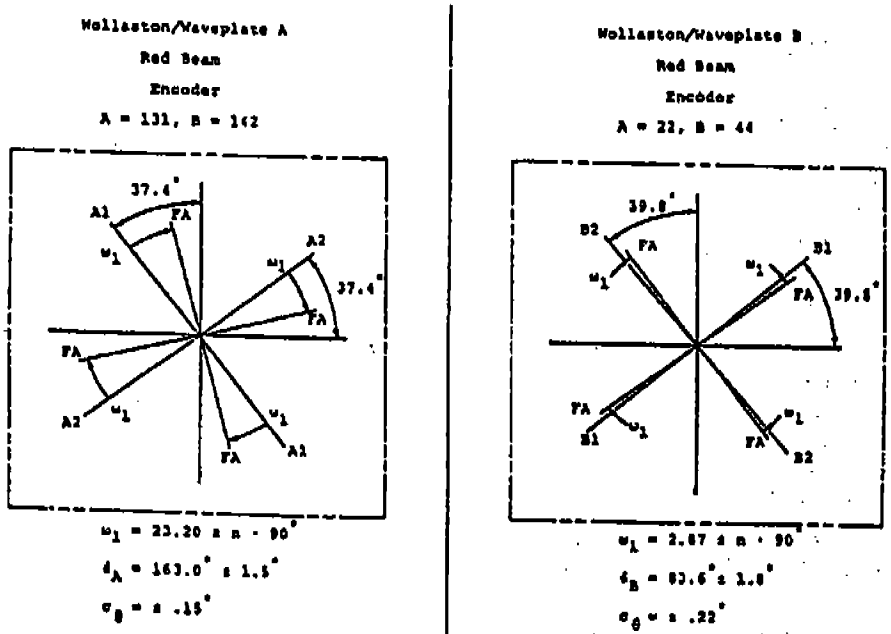

Figure 8.3-4. Diagrams of the Wollaston pass directions and the initial positions of the waveplates that were derived from the operational tests of the polarimeter

accuracy of measurement will be set entirely by photoelectron statistics. This is the case now for most ground-based polarimetry. With the transmission and modulation efficiency of the flight polarimeter determined, and the efficiency of the FOS known, the measurement accuracy can be predicted with a high degree of confidence.

In Table 8.3-2, we have carried through estimates for an AO star with V = 15th magnitude. Its flux is typical of many objects that will be of interest, such as Seyfert nuclei, bright QSO's, BL Lac Objects, the bright knots of M87's jet, magnetic white dwarfs, and AM Her objects. Column 1 gives wavelengths from 1216 to 3000 Å, and column 2 the source flux in ergs/cm^2/Å/sec. Column 3 is the calculated number of photoelectron events per 100 Å bandwidth that will be recorded in an integration going through all 16 waveplate positions in 20 minutes. Some 134.4 seconds are lost to mechanical cycling through 16 rotations of the drum. We have taken account of losses in the HST main optics, in the FOS and polarimeter, and the fact that the digicon can detect only one of the two spectra at any moment. The FOS efficiency is not strongly dependent on resolution; the counts will be somewhat higher when the sapphire dispersing prism is used to cover the region above 1600 Å in one integration.

Columns 4 and 5 give the efficiency for the optimum waveplate at each wavelength and the error in measuring linear polarization; $\sigma(P)$ is given by $\sqrt{2}/\eta\sqrt{N}$, and is the standard deviation of each Q/I and U/I. When appreciable polarization is detected, it is also equal to the error in P, the degree of

TABLE 8.3-2

COUNT RATE AND POLARIZATION ACCURACY FOR AO STAR, V = 15

(1) λ(Å)	(2) log F_λ	(3) Count in 20 minutes in 100 Å Band	(4)		(5)	
			η(P)	σ(P)	η(V)	σ(V)
1216	-14.6	595	.91	6.4%	1.00	5.8%
1500	-14.2	9,500	.76	1.9%	.95	1.5%
2000	-14.1	39,550	.80	0.89%	.96	0.74%
2500	-14.2	78,000	.77	0.66%	.94	0.54%
3000	-14.4	69,500	.85	0.63%	.92	0.58%

polarization. (Errors in P are not gaussian when P is null or weak.) The last two columns give the higher of the two wave-plate efficiencies for V, and the standard deviation in V, also given by $\sqrt{2}/\eta\sqrt{N}$.

We see that the errors in a 20-minute measurement in the 100 Å bandwidth vary from 0.6% to 6% over the range from 3000 to 1216 Å. For some objects with high polarization, this will already be a useful measurement; when higher accuracy is needed, longer exposures and/or wider bands will be required. For example, the band 1500 - 2000 Å could be measured to ~ 0.2% accuracy in a 3-hour integration.

8.4 Instrument-Level Performance

The FOS system level polarimetry measurement data are still under analysis, and will be provided later as an update to this report.

9.0 ACKNOWLEDGEMENTS

Several people contributed to the calibration efforts addressed in this document. The author wishes to thank the many FOS science team members, UCSD programmers, and engineers at MMDA who carried out the measurements described above.

One person stands out as having contributed most to the FOS calibration effort. Dr. George Hartig, now at the STScI, carried out calibrations on the FOS ranging from the original measurements of optical component efficiencies made at JHU around 1980 through the extensive absolute efficiency instrument-level calibrations carried out as late as 1985. He designed the calibration procedures and much of the calibration facilities, carried out the measurements, and analyzed them in significant depth.

Other individuals also contributed greatly to this effort. Richard Allen calibrated the polarization analyzer as a subsystem, and is continuing to analyze the instrument-level polarimetric calibrations. Holland Ford and Anne Kinney continue to improve the target acquisition procedures and the calibration database associated with this important function. Ed Beaver and Gene Strein devoted much effort to measuring the detector efficiency and instrument background performance. Last, but certainly not least, Melanie Terry deserves thanks for the patience and accuracy with which she typed and assembled the several drafts of this rather extensive document.

REFERENCES

Beaver, E. and Harms, R. 1984. "Faint Object Spectrograph Detector Report," April 1984, to STPG.

Ebbets, D. 1985. "Calibration of the HRS Paired-Pulse Effect," ST ScI HRS-CAL/006, January 15, 1985.

Haas, G. and Hunter, W. R. 1970. Applied Optics, 9, 2101.

Heaney, J. B., Herzig, H. and Osantowski, J. F. 1977. Applied Optics, 16, 1886.

Herzig, H. 1984. "Inspection of FOS Optics," September 7, 1984, memo to Code 400.2, GSFC.

Ott, W. R., Bridges, J. M. and Klose, J. Z. 1980. Optics Letters, 5, 225.

Ott, W. R., Behringer and Gieres 1975. Applied Optics, 14, 2121.

Ott, W. R., Fieffe-Prevost and Wiese 1973. Applied Optics, 12, 1618.

Pembroke, R. 1983. "Prism Model in Compilation of JHU Test Results of FOS Optical Components."

Pembroke, R. 1984. "Grazing Mirror Reflectance Calculations," July 25, 1984, letter to R. Harms.

APPENDIX A

DESCRIPTION OF AMBIENT STOS

APPENDIX A

AMBIENT SPACE TELESCOPE OPTICAL SIMULATOR

1. INTRODUCTION

The Ambient Space Telescope Optical Simulator (ASTOS) was designed and built to provide a stable repeatable absolute radiometric calibration of the Faint Object Spectrograph (FOS) over the wavelength range 250 - 850 nm, and under ambient room temperature and atmospheric pressure environments.

The ASTOS consists of three major elements: 1) The structural mount which provides physical support, and proper geometric alignment and interfaces with the FOS, 2) The lamp/diffuser combination that provides the source of illumination for the FOS, and 3) a highly stable power supply for the lamps used.

Figure A-1 is a schematic of the geometrical arrangement of the lamp, diffusing screen, and FOS interface. The ASTOS provides a properly formatted beam with central obscuration to simulate the actual ST capability. Figure A-2 shows a photograph of the actual device. The lamp housing accommodates either a FEL type 1000 W Tungsten lamp provideded by Gamma Scientific, or a FEL type Deuterium lamp, also supplied by Gamma Scientific. Each lamp has its own carefully regulated power supply to provide stable operation and performance. Figure A-3 is a portion of an engineering drawing which illustrates the ASTOS/FOS mounting interface. Special design attention was paid to provide accurate registration and repeatable alignment of the ASTOS for the FOS mounting fixture.

Details of each of the lamps used is provided in following sections. The entire assembly was calibrated at the National Bureau of Standards, Radiometric Physics Division. This calibration was performed both before and after a series of FOS calibrations with the ASTOS, to verify its long term stability.

The reports of those calibrations are also provided here.

In actual operation with the FOS, the lamps were allowed to adequately warm up ($\sim$20 min) before actual data was obtained by FOS. A log was maintained of actual on time usage.

Provision was also made within the ASTOS to house a special polarizing prism. The orientation of this prism could be selected to provide a linearly, polarized continuum source, in position angle increments of 45°.

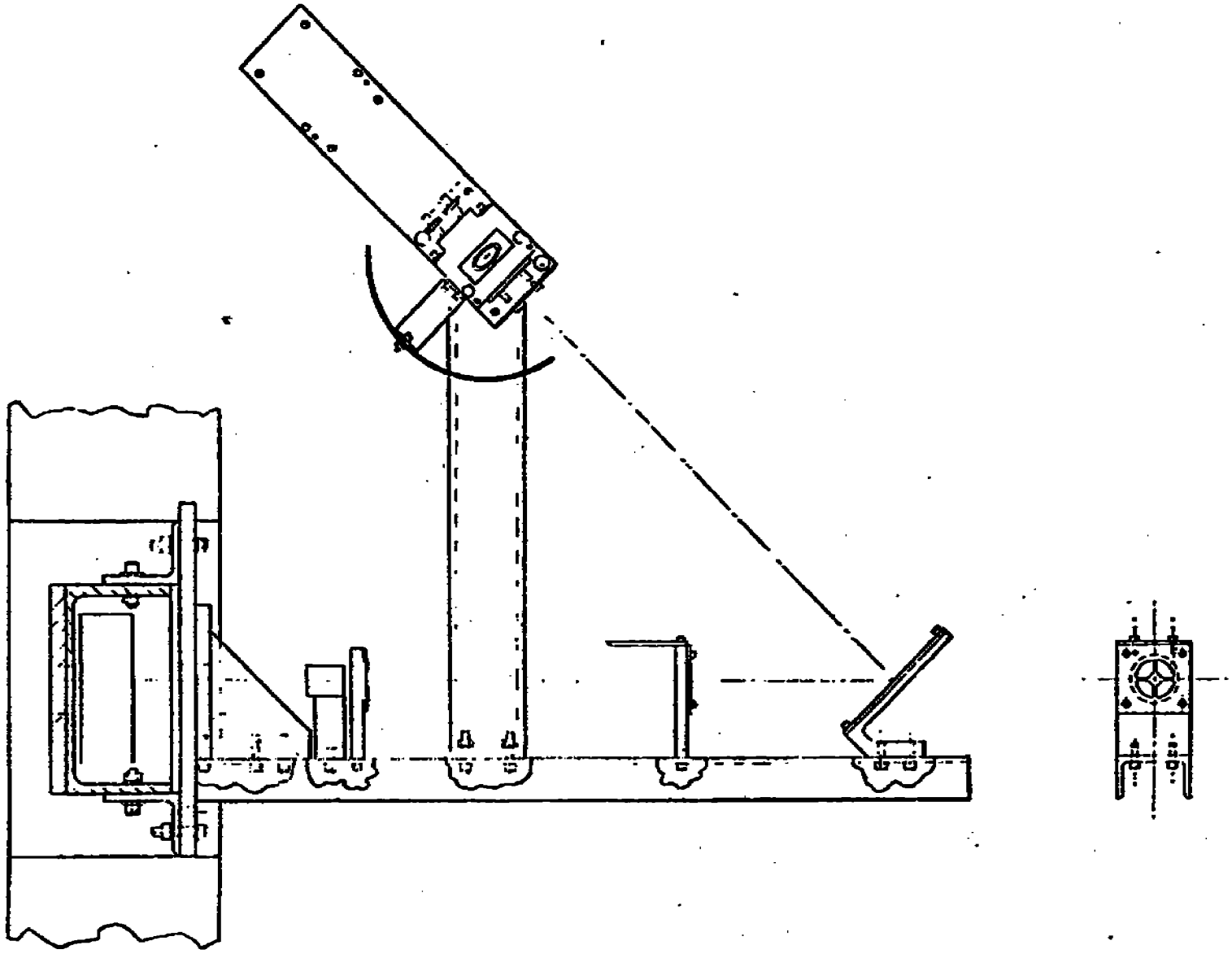

FIGURE A-1 ASTOS CONFIGURATION

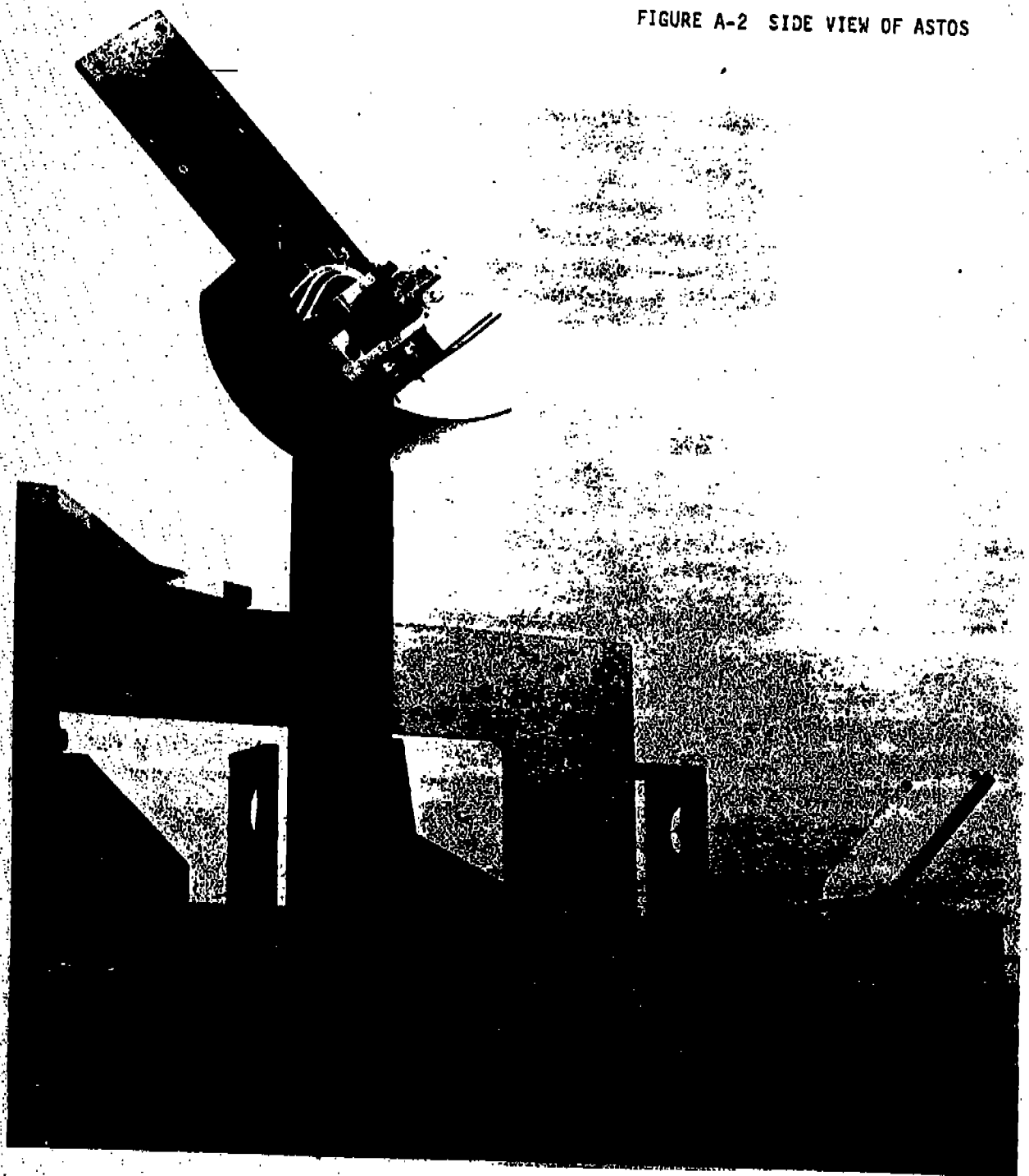

FIGURE A-2 SIDE VIEW OF ASTOS

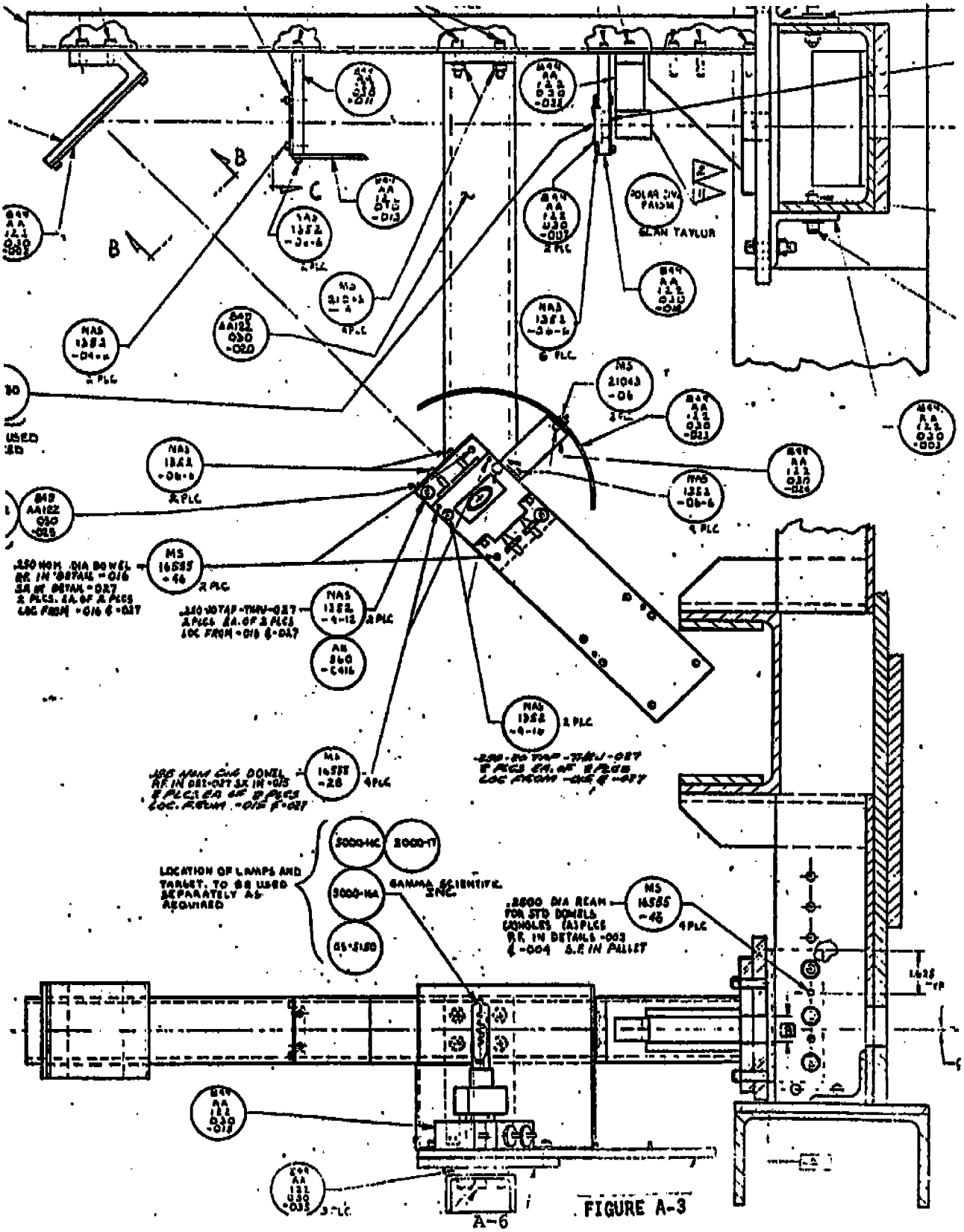
B
C
B
SEAN TAYLOR
USED
LOCATION OF LAMPS AND TARGET. TO BE USED SEPARATELY AS REQUIRED
GAMMA SCIENTIFIC INC.
4 PLC
2 PLC
6 PLC

FIGURE A-3

TUNGSTEN LAMP DESCRIPTION

TUNGSTEN HALOGEN TYPE FEL LAMPS

The tungsten halogen lamp is the principle standard for absolute radiometric calibration. This standard of spectral irradiance consists of a carefully selected and aged lamp with low drift rate, powered by a highly regulated DC supply. The lamp's output is measured at anexact distance (50cm) from it in a carefully defined direction.

A spectral irradiance calibration is performed with the Lamp mounted within a House and Baffle Assembly correctly located on an Optical Bench, and takes into account all interractions and geometry of these two units. The lamp current is measured across a 10 mv/ampere precision calibrated shunt. The voltage is monitored directly at the lamp pins.

This Standard of Spectral Irradiance has become the most accurate and practical reference for measurement of optical radiation.

The Gamma Scientific calibrated tungsten halogen lamp provides state-of-the-art accuracy as a standard of spectral irradiance and is an ideal source to calibrate spectroradiometers, radiometers, and photometers.

The Power Supply is a highly regulated programmable dc supply, which can operate the 1000 watt 8.3 amp lamp. Once the lamp has stabilized thermally, typical random variations in either current or voltage should be less than ±0.01% from one minute to the next.

GAMMA SCIENTIFIC

CALIBRATION REPORT

FOR

FEL TUNGSTEN LAMPS

DEUTERIUM LAMP DESCRIPTION

DESCRIPTION OF THE DEUTERIUM LIGHT SOURCE

The deuterium lamp supplied by Gamma Scientific is a fused silica envelope potted in a special base with two stainless steel pins. The overall dimensions of the lamp are 121 mm high and 22.5 mm between the centers of the two stainless steel pins. Figure 1 shows a cross section of the GS-5150. The lamps inner structure consists of a cathode, anode, and the cover for these electrodes. The envelope is filled with highly pure deuterium to a pressure of several torr. The anode is in the approximate center of the envelope, completely insulated from the other parts of the lamp. A small (approximately 1 mm diameter) aperture is positioned near the front surface of the anode and is designed to pass the entire discharge current, providing a high intensity point source. A special fused silica window is provided in the envelope. The deuterium lamp makes use of arc discharge. Figures 2 and 3 show the discharge mechanism for this lamp operation. As shown in Figure 2, when two flat plate electrodes, placed in a gas environment and separated by distance D, have a voltage applied to them, the negative electrode becomes the cathode, the positive electrode the anode, and current flows in the circuit shown. This flow is due to residual ions excited in the gas by the photoelectric effect, cosmic rays or radioactive matter. As the applied voltage is increased, the current begins to increase in proportion to the voltage from A to B, as shown in Figure 3. While the slope (coefficient of proportionality) depends on ion and electron density and movement, further increase in voltage beyond the point B, results in a saturation condition up to the point C. This occurs when all of the supplied electrons are being transported. If the applied voltage is increased still further, a sharp increase in current is seen as from point C to point D in Figure 3. This increase occurs when sufficient energy is imparted to the gas molecules to cause electrons to break away due to collisions. This is the discharge (breakdown) mechanism.

OUTLINE DRAWING OF

GAMMA SCIENTIFIC

GS-5150 CALIBRATED UV DEUTERIUM SOURCE

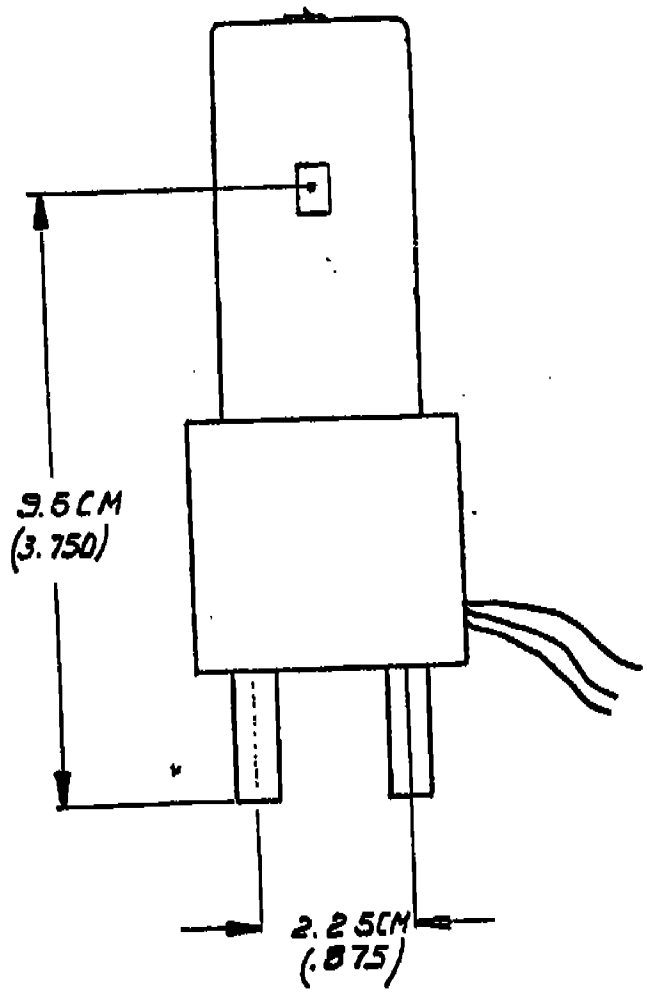

Figure 1

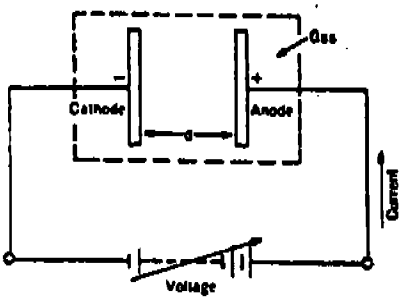

Flat plate electrodes

Figure 2

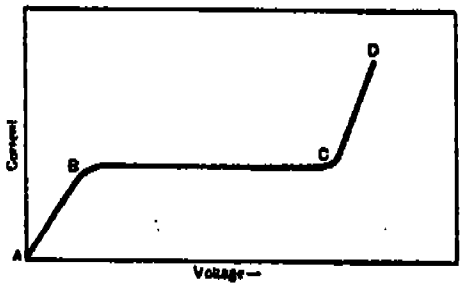

Applied voltage and discharge current of flat plate electrodes

Figure 3

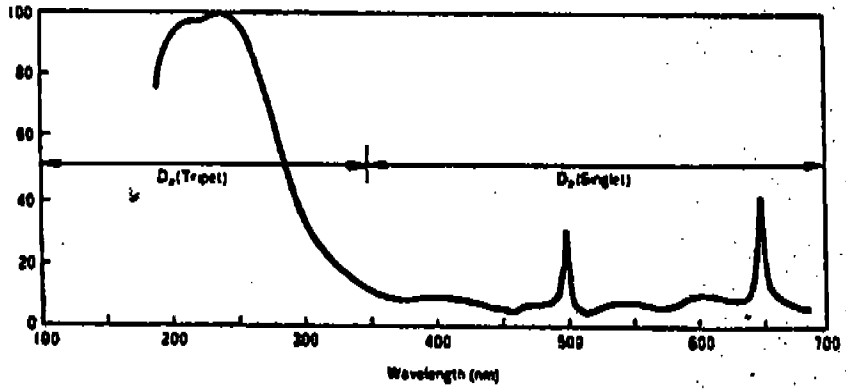

Radiant intensity spectral distribution (Hamamatsu type L544)

Figure 4

If the proper voltage is applied to a low pressure discharge lamp with a series resistor, stable gas discharge will be achieved under suitable conditions for discharge. This type of discharge is termed "glow discharge". When the discharge current is increased, the cathode temperature rises due to the effect of colliding positive ions bringing upon thermionic emission of electrons and a resulting decrease in steepness of the normally pronounced cathode fall, resulting in a potential sufficient to allow creation of additional free electrons - the condition known as arc discharge. Figure 4 shows the Radiant Intensity Spectral Distribution for a deuterium lamp. For sparcely populated samples, the deuterium spectrum exhibits singlet radiation in the visible region and in the Lyman Region under low energy excitation. As shown in Figure 4, the radiant intensity spectral distribution of a deuterium lamp reaches its highest level in the wavelength range 220-230 nm, falling off at longer wavelengths.

Electrical Requirement

The GS-5150 Deuterium Lamp requires 10 Volts from the GS-5120 Power Supply. The radiant intensity of the deuterium lamp is nearly proportional to the lamp current, and thus power supply regulation is an important factor in determining the output level stability. Thus a $\pm$0.1% output level stability requires a $\pm$0.1% power supply regulation. The GS-5120 Power Supply meets this requirement. The GS-5120 is a constant current power supply for deuterium lamps commonly used in continuous UV light sources. The automatic circuit function will offer easy lamp starting and stable operation. All lamps with 2.5 and 10 Volt type filaments can be operated with the GS-5120.

This includes most lamps from a wide variety of manufacturers such as Hamamatsu, Westinghouse, Sylvania, Quartz Lamper and Cathodeon.

Kinematic Socket and Alignment Jig

The deuterium light source consists of the kinematic socket, the GS-5150 Lamp, the GS-5120 Power Supply and is shown in Figure 5 when correctly connected. The kinematic socket and alignment jig and an FEL 1000 Watt Tungsten Halogen Lamp are shown in Figure 6. As shown in Figure 1 for the deuterium lamp, the stainless steel posts are not connected to the lamp directly, but are used only for alignment of the lamp. The power for the lamp is supplied to the lamp by three wires extending from the rear of the base. The lamp is aged for 100 hours at 300 milliamperes, then oriented and potted in the bi-post base, which is aligned with a spectroradiometer according to the alignment instructions given below in the Operation Section. The lamp orientation is chosen so as to minimize the variations in the radiation field about the aligned position at 250 nm. The deuterium lamp is oriented so that the optical axis of the radiometer passes perpendicularly to a plane defined by the front surfaces of the lamp base posts. Orientation of this plane is set in pitch-and-yaw to within $\pm 1^{o}$ (approximately 2% flux change). This defined plane is set 50 cm from the entrance aperture of the radiometer. The optical axis also passes midway between the posts and 9.5 cm above the bottom of the posts. The deuterium lamp may be inserted in the kinematic socket by tightening the spring loaded knurled screws and inserting the two pins of the lamp base into the socket until they touch the bottom of the socket. The alignment of the kinematic socket (Model 5000-17) is facilitated by using the alignment jig (Model 5000-18). The alignment jig consists of two long rods potted into a base similar to the FEL lamp shown in Figure 6, but with the rods extended up out of the epoxy block as well as below the block. A piece of glass is fitted between the parallel rods with one face in the plane that is tangent to one side of the rods. On the front surface of the glass is a fiducial mark (a cross). The center of this fiducial mark is 9.5 cm above the end of the base of the pins and centered on the optical axis midway between two long rods. The kinematic socket should be mounted on a table which will allow it to be adjusted in pitch-and-yaw. In addition, unless the radiometer has x and y motion, the kinematic socket should include this as well. Since

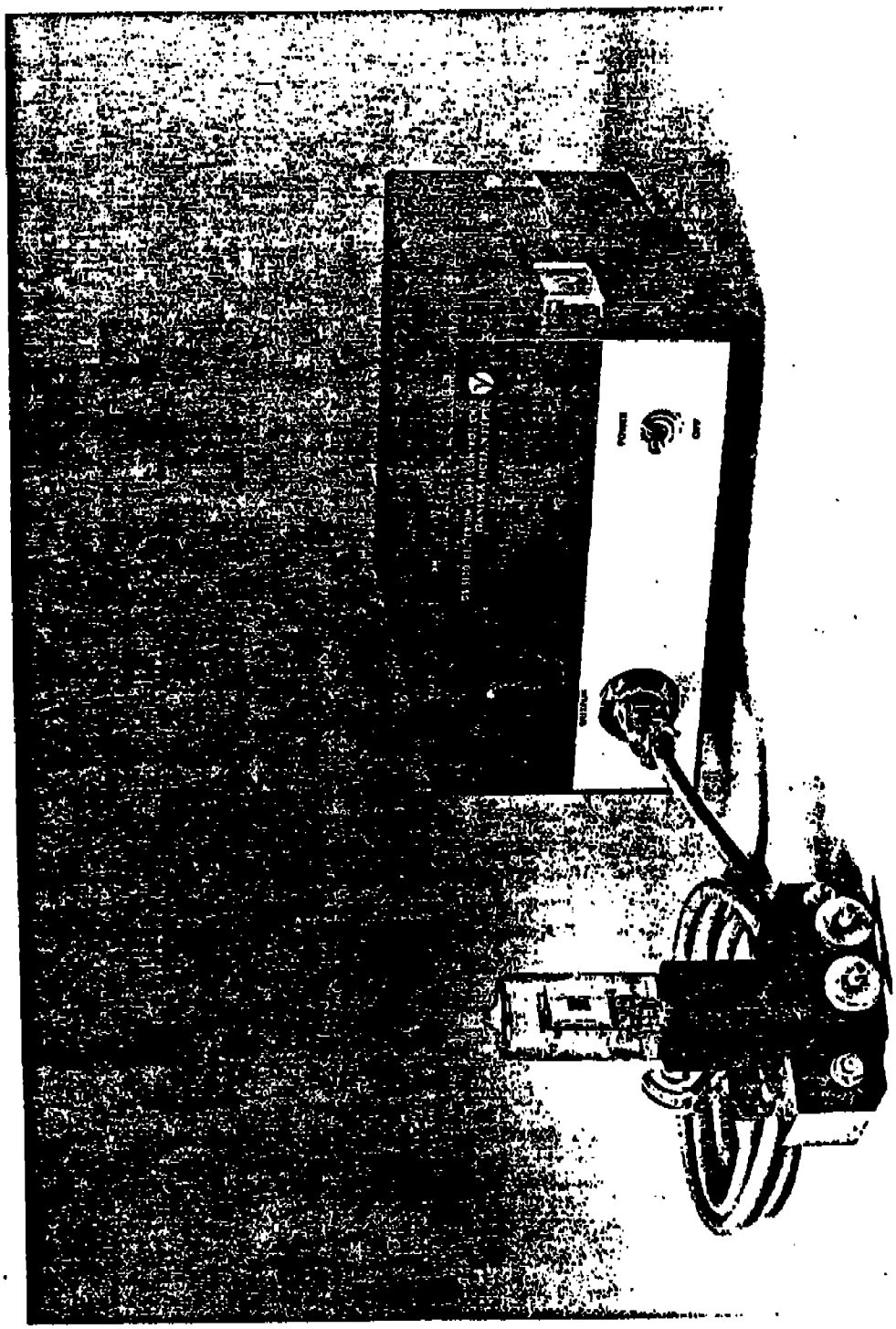

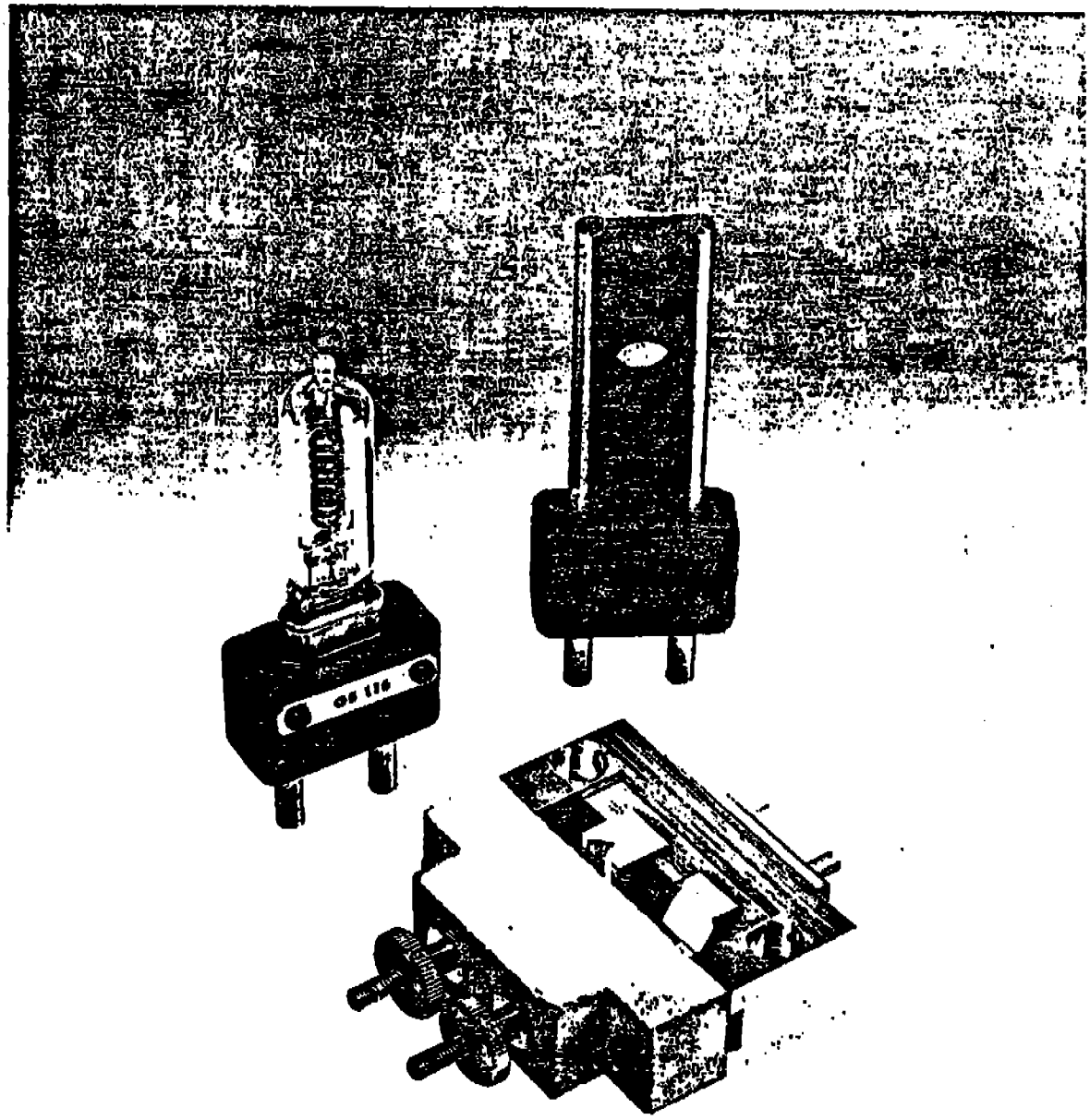

Figure 6

the radiation beam from the deuterium lamp is very directional, the necessity of maintaining correct adjustment of the kinematic socket using this alignment jig is paramount to insure that irradiance values given are correct.

NEW D_2 LAMP STANDARDS OF SPECTRAL IRRADIANCE

D. A. McSparron

For the past four years, NBS has issued D_2 lamp standards of spectral irradiance covering the spectral range 200-350 nm (ORN #14, March 1976). The uncertainty has been estimated to be 6% absolute and 2-3% in relative spectral output. Further, NBS has strongly urged customers also to obtain a tungsten, quartz-halogen, type FEL lamp standard of spectral irradiance and normalize the reported D_2 spectral irradiance values to the FEL values at the time of measurement. In the past two years a disturbing number of problems with the issued D_2 lamps (manufacturer A) have been reported by customers. Most of the reported problems relate to a "shelf effect". Of the approximately 50 issued lamps, 10-16% have been observed to shift in absolute output by 10-25% after sitting, unburned on a shelf for 2-6 months. In all but one case, the observed shifts were in absolute output only, i.e. the relative spectral output held constant to 2-3%. Thus, if customers were following the recommended procedure of normalizing against a type FEL standard, the reported uncertainties would still hold. The one exception noted above involved a lamp hand-carried to another government agency in the Washington, D.C. area, and later rechecked at NBS. The observed shifts in relative spectrum was on the order of 5-10%, and even this case would have been revealed if the recommended normalization against an FEL had been used at more than one wavelength (250 nm and 300 nm are being recommended). The causes of these shifts have not been definitively determined. However, one or more of the following effects are believed to be involved: restriking of the arc at different points on the heater filament, impurities in the tungsten heater filament, outgassing of the lamp envelop, selective window contamination, and slow gas leaks.

Obviously, the issued lamps have been far from ideal as standards. After discussions with manufacturers and customers, and limited testing at NBS, a new D_2 lamp has been chosen for issuance (manufacturer B). As before, the new lamp has been mounted in a medium bipost base with the optic axis 9.5 cm above the bottom of the base pins. This mounting allows easy optical alignment and preserves compatibility with the type FEL standards. The electrical operating circuit is identical, although there are minor differences in the electrical parameters of the heater circuit (10 volts, 0.8 amps for the new lamps vs. 4 volts, 5 amps for the old). The spectral irradiance values are approximately the same for both types. NBS testing of the new lamps has covered about 6 months. No "shelf effects" have been observed. However, it should be emphasized that the problems with the lamps from manufacturer A did not reveal themselves until several years experience had been gained. As of July, 1980 NBS will supply D_2 lamps from manufacturer B. Customers are strongly urged to use the recommended normalization procedure against an FEL. Customers are also urged to report promptly any adverse experience with the new lamps to D. McSparron (telephone: (301) 921-3613

EG&G GAMMA SCIENTIFIC

EG&G GAMMA SCIENTIFIC INCORPORATED. 3777 RUFFIN ROAD SAN DIEGO CALIFORNIA 92123 • TEL (714) 279-8034

REPORT OF CALIBRATION

MODEL Gs5150

SERIAL NO. DL 116

ON 16 August 1982 the Spectral Irradiance of this lamp in Microwatts/cm^2·nm at a distance of 50.0 cm at right angles to the plane of the front of the bi-post pins on the base in a line halfway between the pins and 9.5 cm above their bottoms was determined as given below.

200	4.2984E-02	300	1.6843E-02
205	4.1275E-02	305	1.6078E-02
210	3.9187E-02	310	1.4734E-02
215	3.6234E-02	315	1.3842E-02
220	3.6596E-02	320	1.3318E-02
225	3.7700E-02	325	1.2942E-02
230	3.9678E-02	330	1.2160E-02
235	4.1784E-02	335	1.1417E-02
240	4.1838E-02	340	1.0805E-02
245	3.9122E-02	345	1.0262E-02
250	3.6606E-02	350	9.6382E-03
255	3.4403E-02	355	9.0565E-03
260	3.1372E-02	360	8.3725E-03
265	2.9596E-02	365	7.8458E-03
270	2.7172E-02	370	7.4841E-03
275	2.4907E-02	375	7.1700E-03
280	2.2956E-02	380	6.9952E-03
285	2.1237E-02	385	6.3808E-03
290	1.9659E-02	390	6.0788E-03
295	1.8174E-02	395	5.8317E-03
		400	5.6997E-03

DONALD M. WEBB
QUALITY ASSURANCE MANAGER

EG&G GAMMA SCIENTIFIC
EG&G GAMMA SCIENTIFIC INCORPORATED, 3777 RUFFIN ROAD, SAN DIEGO, CALIFORNIA 92123 • TEL (714) 279-8034

REPORT OF CALIBRATION

MODEL GS5150

SERIAL NO. DL 117

ON 16 August 1982 the Spectral Irradiance of this lamp in Microwatts/cm^2·nm at a distance of 50.0 cm at right angles to the plane of the front of the bi-post pins on the base in a line halfway between the pins and 9.5 cm above their bottoms was determined as given below.

WL	Value
200	5.5344E-02
205	5.0699E-02
210	4.6621E-02
215	4.3304E-02
220	4.2818E-02
225	4.4365E-02
230	4.5824E-02
235	4.8294E-02
240	4.8040E-02
245	4.5555E-02
250	4.1765E-02
255	3.8941E-02
260	3.5752E-02
265	3.3386E-02
270	illegible
275	illegible
280	illegible
285	illegible
290	illegible
295	illegible
300	1.8751E-02
305	1.7913E-02
310	1.6228E-02
315	1.5239E-02
320	1.4696E-02
325	1.4365E-02
330	1.3474E-02
335	1.2508E-02
340	1.2049E-02
345	1.1291E-02
350	1.0605E-02
355	9.9608E-03
360	9.3118E-03
365	8.6914E-03
370	8.2621E-03
375	7.7078E-03
380	7.6996E-03
385	7.0453E-03
390	6.6798E-03
395	6.5064E-03
400	6.2399E-03

DONALD M. WEBB
QUALITY ASSURANCE MANAGER

NBS CALIBRATION

REPORT FOR ASTOS

FORM NBS-443
(REV. 11-63)

U.S. DEPARTMENT OF COMMERCE
NATIONAL BUREAU OF STANDARDS
WASHINGTON, D.C. 20234

REPORT OF CALIBRATION

of
FOS Source

Supplied to:
Martin Marietta Corporation
Denver, Colorado

(See your Purchase Agreement number XH2-135220, dated July 16, 1982.)

I. Material

One specially designed irradiance test fixture was supplied to NBS by the Martin Marietta Corporation. The fixture was designed to be used as a calibration source for the Faint Object Spectrograph used in the Space Telescope. In the remainder of this report, the fixture will be referred to as the FOS source. Included with the FOS source were two FEL lamps designated GS-179 and GS-180, two deuterium lamps designated DL116 and DL117, and three barium sulphate diffusers designated #1, #2, and #3 (#1 was used only for alignment).

II. Calibration

A. Method

The measurements were done in two parts. From 300 nm to 850 nm the spectral irradiance was measured directly. Below 300 nm the spectral irradiance of the FOS source was too low to measure accurately using the irradiance measurement mode. Spectral radiance measurements were made and the spectral irradiance was calculated from the geometry of the optical system.

The spectral irradiance measurements were performed using a spectroradiometer with a 3.5 cm diameter integrating sphere with a 7.5 mm diameter entrance aperture to collect the flux from the source. Average spectral irradiances of the test source over the spectral slit width of the instrument were determined by spectral comparison with a previously calibrated 1000-watt type FEL lamp standard of spectral irradiance designated F-30. The spectral slit width of the radiometer varied from approximately 5 nm at 300 nm to 7 nm at 850 nm.

Below 300 nm the spectral radiance was measured at the specified location for which the irradiance was desired (point A in figure 1). The spectral radiance was determined by a spectral comparison of the test source with a previously calibrated lamp standard of spectral radiance designated Q66. The solid angle of the FOS source was calculated from the geometry of the test fixture with the obscuration aperture in place, and this number was multiplied by the spectral radiance to yield the spectral irradiance. The solid angle of the FOS source was determined to be 1.16E-3 steradians.

Measurements were made using both FEL lamps and the #2 and #3 diffusers from 250 nm to 850 nm and using both deuterium lamps and the #2 and #3 diffusers from 200 nm to 300 nm. Lower level measurements were made in the radiance mode using GS-179 and the #2 diffuser from 350 nm to 850 nm.

B. Conditions

For the spectral irradiance measurements the FOS source was oriented (see figure 1) so that the horizontal optical axis of the spectroradiometer passed through the center of the opening in the detector support mount at point B, through the pinhole on the obscuration aperture at point C, and to the center of the cross scribed on diffuser #1 (used only for alignment) at point D. The FOS source was translated horizontally until point A, located 36.1 cm from point B and 79.4 cm from point C, was positioned at the center of the opening of the receiving aperture of the integrating sphere.

For the spectral radiance measurements the FOS source was again oriented so that the optical axis of the spectroradiometer passed through points B, C, and D. It was translated horizontally so that the point A was imaged onto the entrance slits of the monochromator. The detector support mount, the filter mount, and the obscuration aperture were removed before the spectral radiance measurements were made. The solid angle seen by the spectroradiometer was determined to be approximately 0.645E-3 steradians.

All lamps were operated at the same current for both the spectral irradiance and the spectral radiance measurements. Both FEL lamps, GS-179 and GS-180, were operated at a power supply dial setting of 8.011 which corresponded to a lamp current of 8.000 amperes. Both deuterium lamps, DL116 and DL 117, were operated at the set point current determined by the

deuterium lamp power supply (lamp current was not measured). Lamp GS-179 was also operated at a power supply dial setting of 6.511 to give a lower output level.

III. Results

Tables I through V give the spectral irradiance of the FOS source at point A (see figure 1) for the various combinations of lamps and diffusers. Table VI gives the uncertainty estimate in the reported spectral irradiances. The largest contributor to the uncertainty was the precision in the spectral comparison measurements of the FOS source to the standard lamps.

Prepared by:

James H. Walker
Radiometric Physics Division
Center for Radiation Research

Approved by:

Donald A. McSparron

Donald A. McSparron
Radiometric Physics Division
Center for Radiation Research

TABLE I

SPECTRAL IRRADIANCE OF FOS SOURCE
WITH LAMP GS-179 AT 8.011 DIAL SETTING (8.000 AMPERES)

WAVELENGTH (NM)	SPECTRAL IRRADIANCE WITH DIFFUSER #2 (W CM**-3)	SPECTRAL IRRADIANCE WITH DIFFUSER #3 (W CM**-3)
250	5.92E-05	6.07E-05
260	1.09E-04	1.08E-04
270	1.83E-04	1.82E-04
280	2.85E-04	2.85E-04
290	4.28E-04	4.28E-04
300	6.28E-04	6.31E-04
325	1.42E-03	1.44E-03
350	2.76E-03	2.78E-03
400	7.55E-03	7.54E-03
450	1.52E-02	1.52E-02
500	2.53E-02	2.52E-02
550	3.59E-02	3.58E-02
600	4.71E-02	4.68E-02
654.6	5.74E-02	5.73E-02
700	6.44E-02	6.45E-02
750	7.14E-02	7.13E-02
800	7.59E-02	7.58E-02
850	7.89E-02	8.14E-02

TABLE II

SPECTRAL IRRADIANCE OF FOS SOURCE
WITH LAMP GS-180 AT 8.011 DIAL SETTING (8.000 AMPERES)

WAVELENGTH (NM)	SPECTRAL IRRADIANCE WITH DIFFUSER #2 (W CM^-3)	SPECTRAL IRRADIANCE WITH DIFFUSER #3 (W CM^-3)
250	6.47E-05	6.46E-05
260	1.13E-04	1.13E-04
270	1.91E-04	1.90E-04
280	2.97E-04	2.96E-04
290	4.47E-04	4.43E-04
300	6.52E-04	6.51E-04
325	1.47E-03	1.47E-03
350	2.79E-03	2.87E-03
400	7.74E-03	7.76E-03
450	1.56E-02	1.56E-02
500	2.56E-02	2.57E-02
550	3.67E-02	3.66E-02
600	4.77E-02	4.78E-02
654.6	5.86E-02	5.83E-02
700	6.55E-02	6.56E-02
750	7.24E-02	7.23E-02
800	7.61E-02	7.69E-02
850	8.04E-02	7.98E-02

TABLE III

SPECTRAL IRRADIANCE OF FOS SOURCE
WITH LAMP DL116 AT OPERATING CURRENT

WAVELENGTH (NM)	SPECTRAL IRRADIANCE WITH DIFFUSER #2 (W CM**-3)	SPECTRAL IRRADIANCE WITH DIFFUSER #3 (W CM**-3)
200	4.53E-05	6.19E-05
210	8.56E-05	9.09E-05
220	9.81E-05	1.03E-04
230	1.16E-04	1.20E-04
240	1.21E-04	1.22E-04
250	1.11E-04	1.11E-04
300	5.29E-05	5.39E-05

TABLE IV

SPECTRAL IRRADIANCE OF FOS SOURCE
WITH LAMP DL117 AT OPERATING CURRENT

WAVELENGTH (NM)	SPECTRAL IRRADIANCE WITH DIFFUSER #2 (W CM'-3)	SPECTRAL IRRADIANCE WITH DIFFUSER #3 (W CM'-3)
200	8.95E-05	1.08E-04
210	1.15E-04	1.26E-04
220	1.22E-04	1.32E-04
230	1.40E-04	1.49E-04
240	1.43E-04	1.49E-04
250	1.31E-04	1.36E-04
300	6.13E-05	6.32E-05

TABLE V

SPECTRAL IRRADIANCE OF FOS SOURCE
WITH LAMP GS-179 AT 6.511 DIAL SETTING

WAVELENGTH (NM)	SPECTRAL IRRADIANCE WITH DIFFUSER #2 (W CM**-3)
350	3.88E-04
450	3.19E-03
555	1.04E-02
654.6	1.95E-02
850	2.73E-02

TABLE VI

UNCERTAINTY ESTIMATE IN
REPORTED SPECTRAL IRRADIANCES

WAVELENGTH (NM)	UNCERTAINTY (%)
200	23
210	18
250	8
350	7
454.6	5
850	7

FOS Source

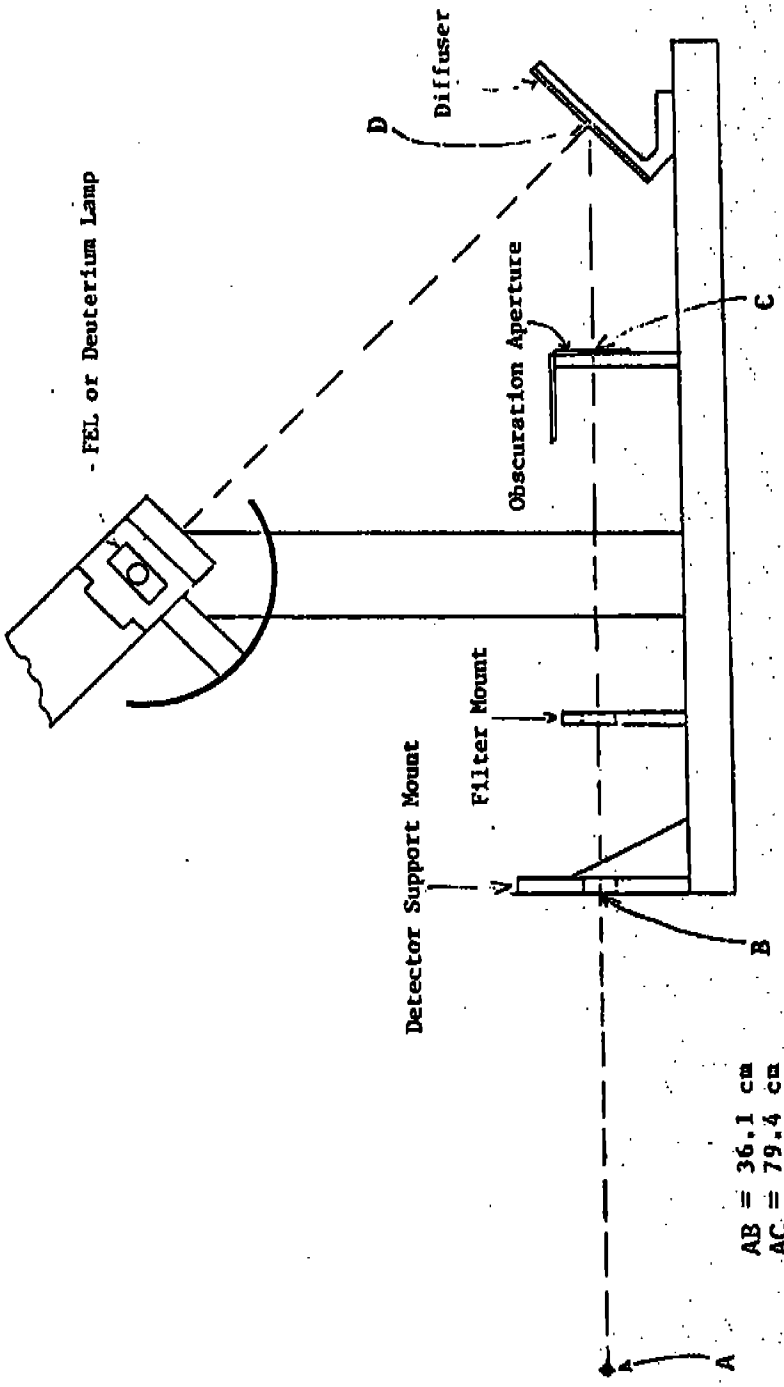

FIG. 1 FOS Source

APPENDIX B

DESCRIPTION OF VACUUM STOS

APPENDIX - B

VACUUM SPACE TELESCOPE OPTICAL SIMULATOR

INTRODUCTION

The Vacuum Space Telescope Optical Simulator (VSTOS), has been designed and built to provide the Faint Object Spectrograph (FOS) with an absolute radiometric calibration standard. The VSTOS is a complex unit which houses a series of five UV line and continuum lamps which are mounted on a stepper motor-driven rotatable carousel. The lamps can be remotely commanded into position to illuminate an inverted Cassegrain optical system which, inturn, illuminates the FOS aperture with a properly formatted, centrally obscured, F/24 optical beam, that simulates Space Telescope optical imaging performance.

This unit is mounted on a platform structure, and enclosed with a hemispherical shroud, as illustrated in Figure B-1. The entire assembly is structurally mounted and aligned with the FOS support fixture to provide proper illumination onto the FOS aperture focal plane. An external controller unit contains an array of switches which select the appropriate lamp to be used, and positions it to the optical feed assembly. Separate power supplies are used to operate each lamp, in conjunction with the controller box.

In practice the VSTOS provides a stable array of line and continuum UV sources which have been used to provide an absolute radiometric calibration of the FOS over the wavelength range 114 to 350 μm.

A small vacuum chamber was refurbished in order to provide a vacuum enclosure by which the VSTOS could be calibrated at the National Bureau of Standards. Details of this calibration, and the results are included as part of Appendix C of this report.

For FOS calibration, the entire unit was installed, integrated, and aligned with the FOS by means of its mounting interface. The combination of FOS and the VSTOS were placed in the large Thermal Vacuum (T/V) chamber at MMDA, for operation and use with FOS. Absolute radiometric calibration of FOS was successfully performed during several (T/V) tests conducted in 1983 and 1984. Further details on the lamps and power supplies are included here for reference, as well as the NBS reports of the VSTOS calibration results.

Figures B-2 thru B-6 illustrates the VSTOS Carosel, baseplate and optical system, as well as the Vacuum chamber used for its calibration at NBS. Figures B-7 and B-8 show the Quantatec continuum lamp configuration and power supply/controller, respectively. Figure B-9 shows the spectral radiance distribution for the various Quantatec lamps. Finalley, Figure B-10 illustrates the configuration of the Resonance LTD. Argon lamp used in the VSTOS.

The line sources used, the PtCrNe hollow cathode lamps built by Westinghouse, are described separately in a Johns Hopkins University Report, Davidsen et al JHU report,1983.

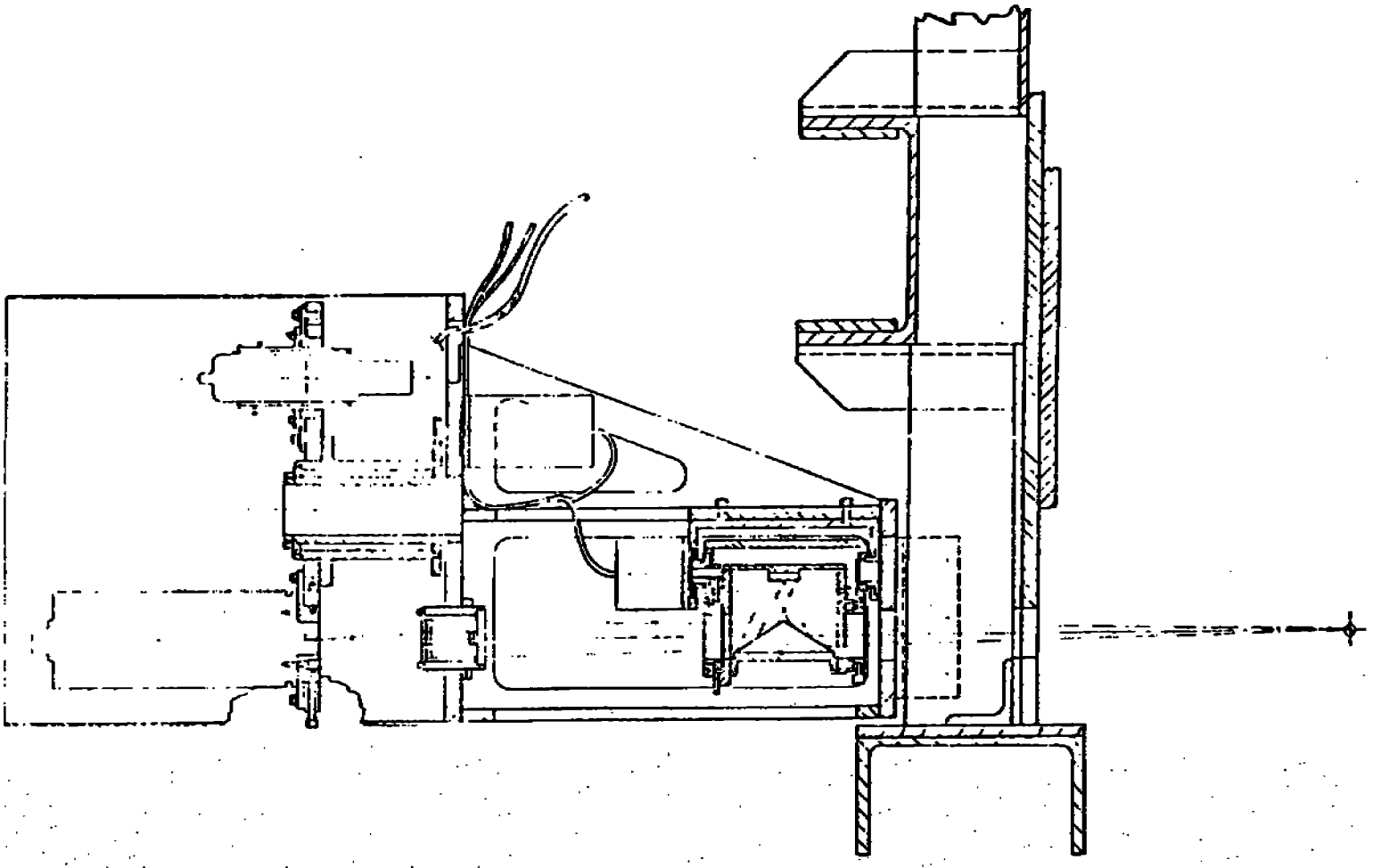

FIGURE B-1 VSTOS CONFIGURATION

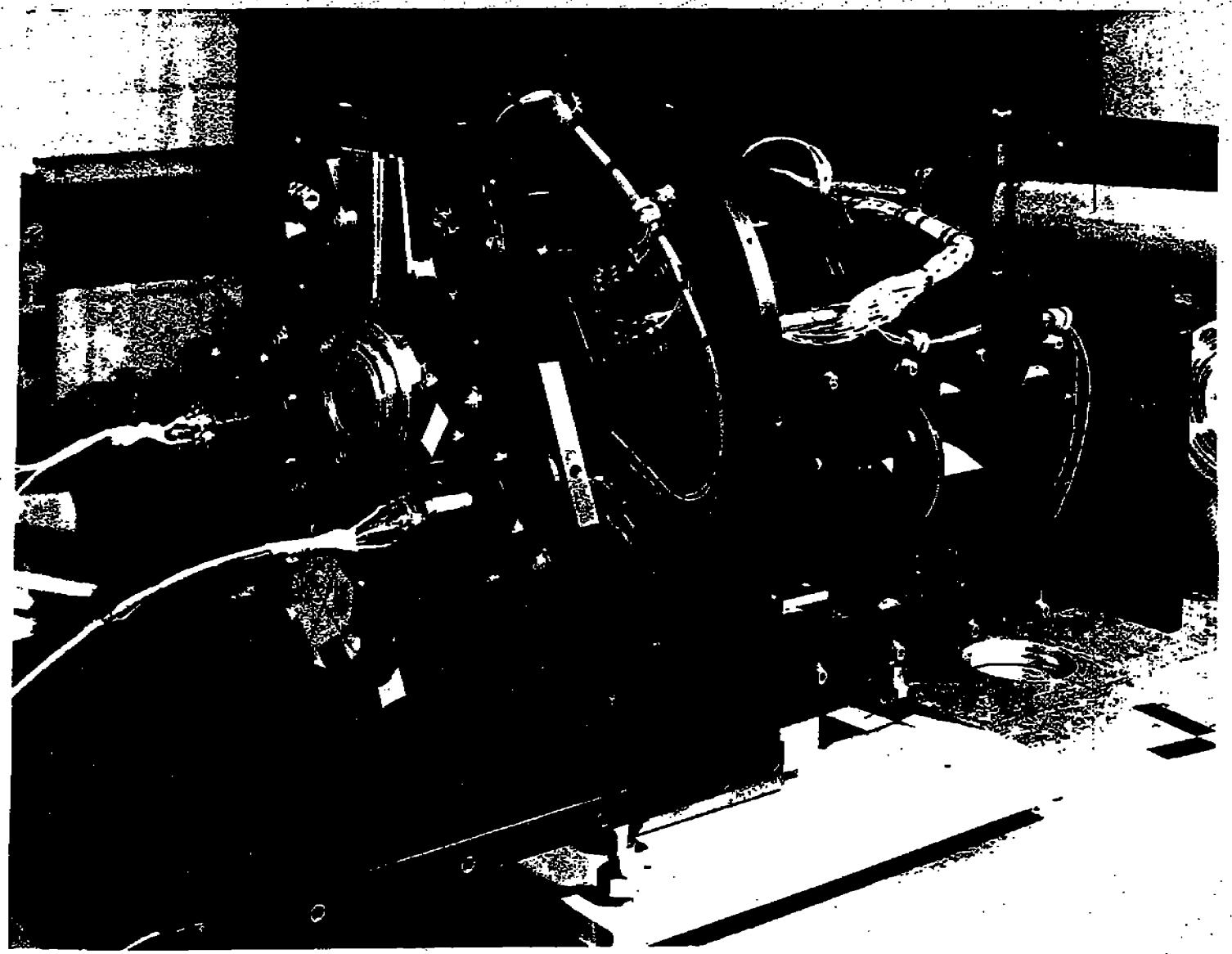

FIGURE B-3 REAR VIEW OF VSTOS

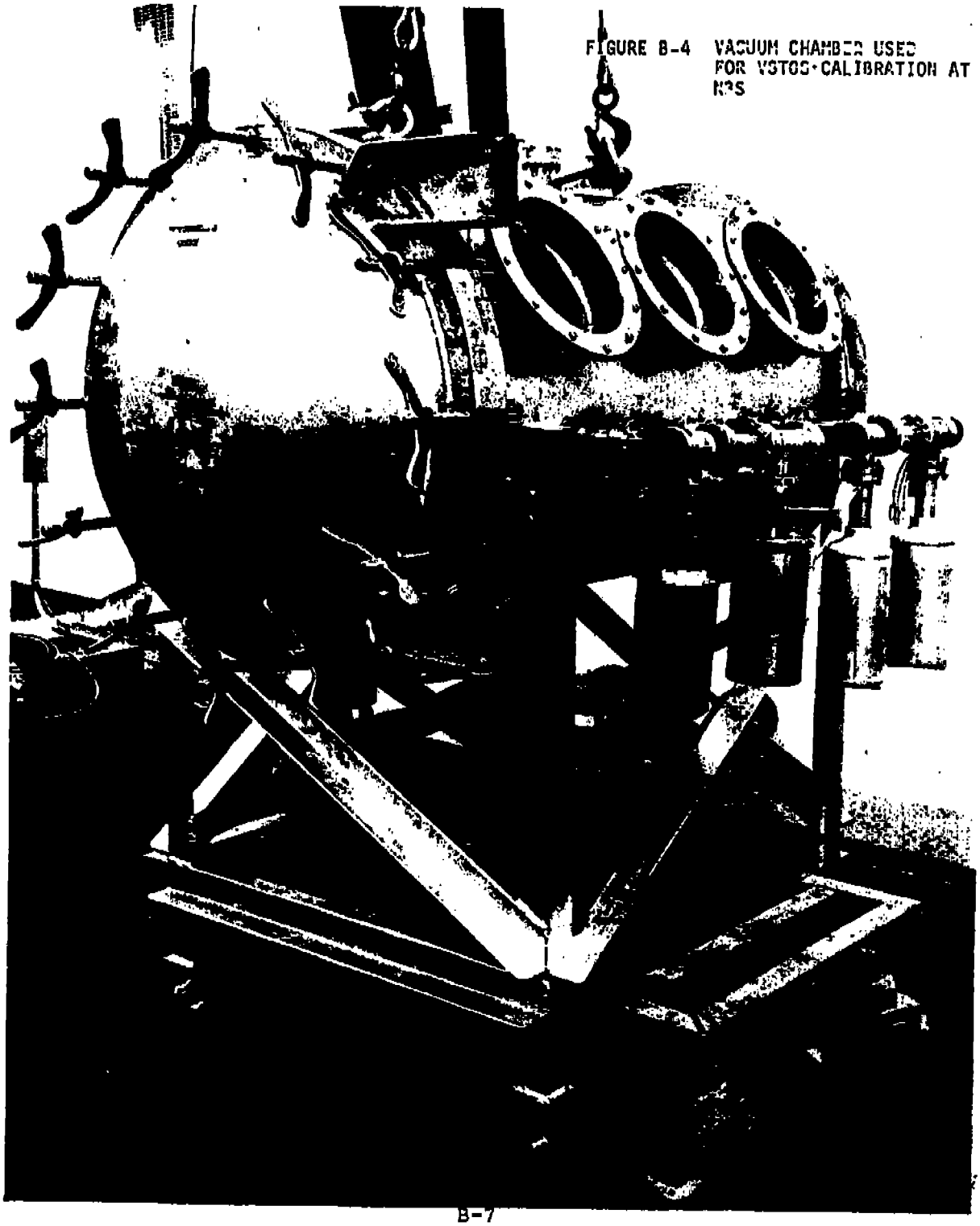

FIGURE B-4 VACUUM CHAMBER USED FOR VSTOS CALIBRATION AT KSC

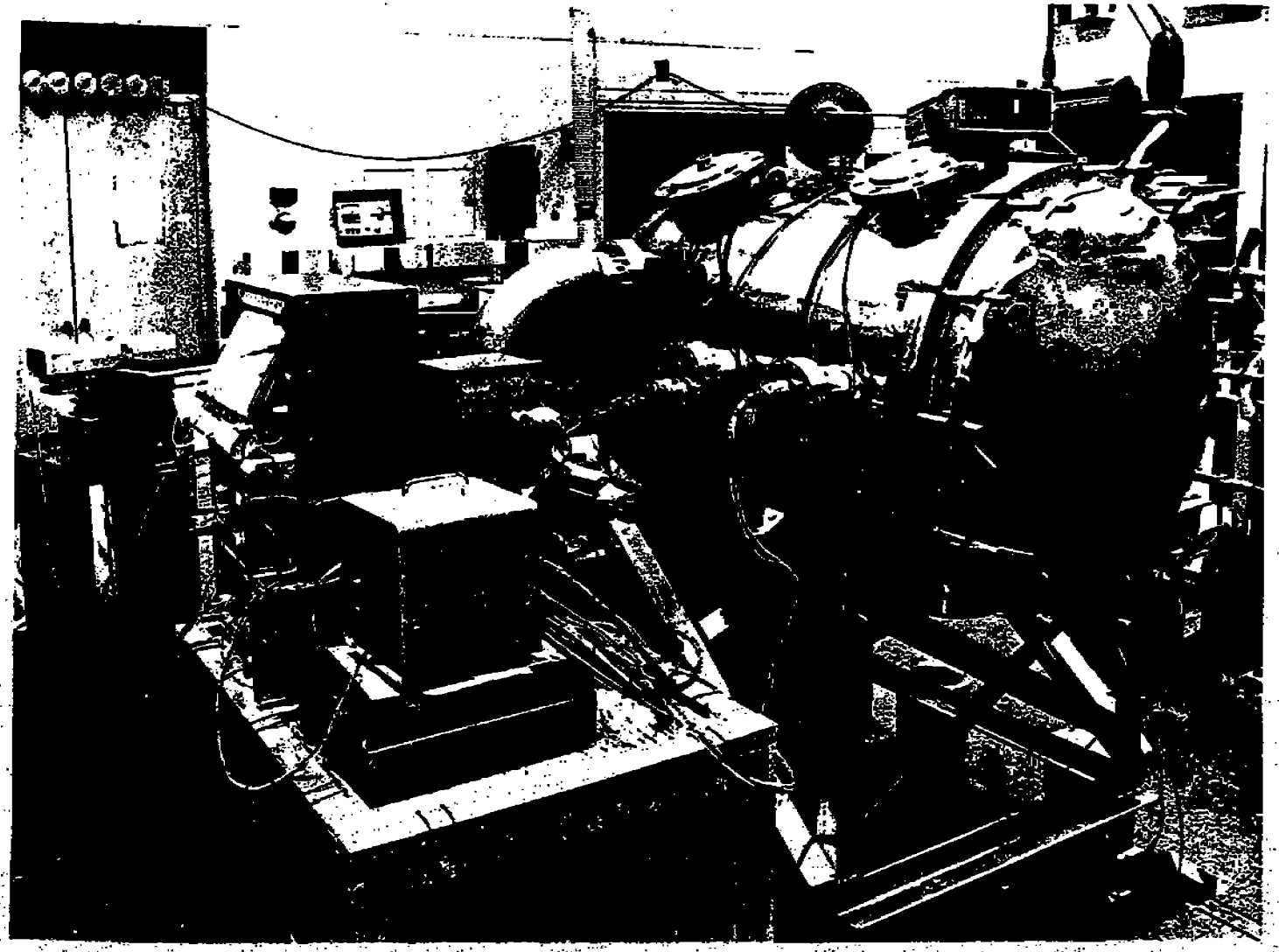

FIGURE B-5 REAR VIEW OF VSTOS VACUUM CHAMBER AT NBS CALIBRATION

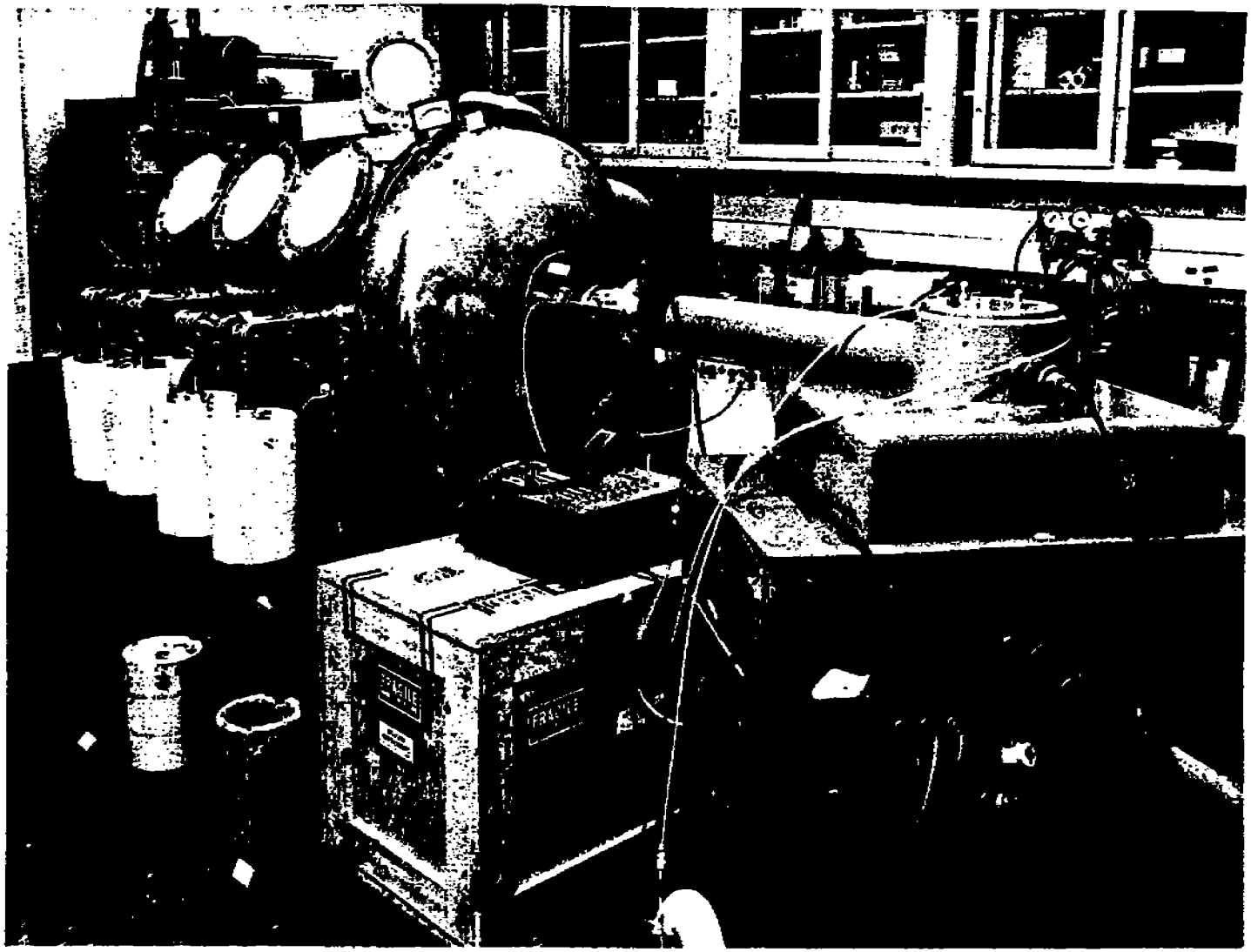

FIGURE B-6 NBS MONOCHROMATOR VIEW OF VACUUM CHAMBER USED FOR VSTOS CALIBRATION

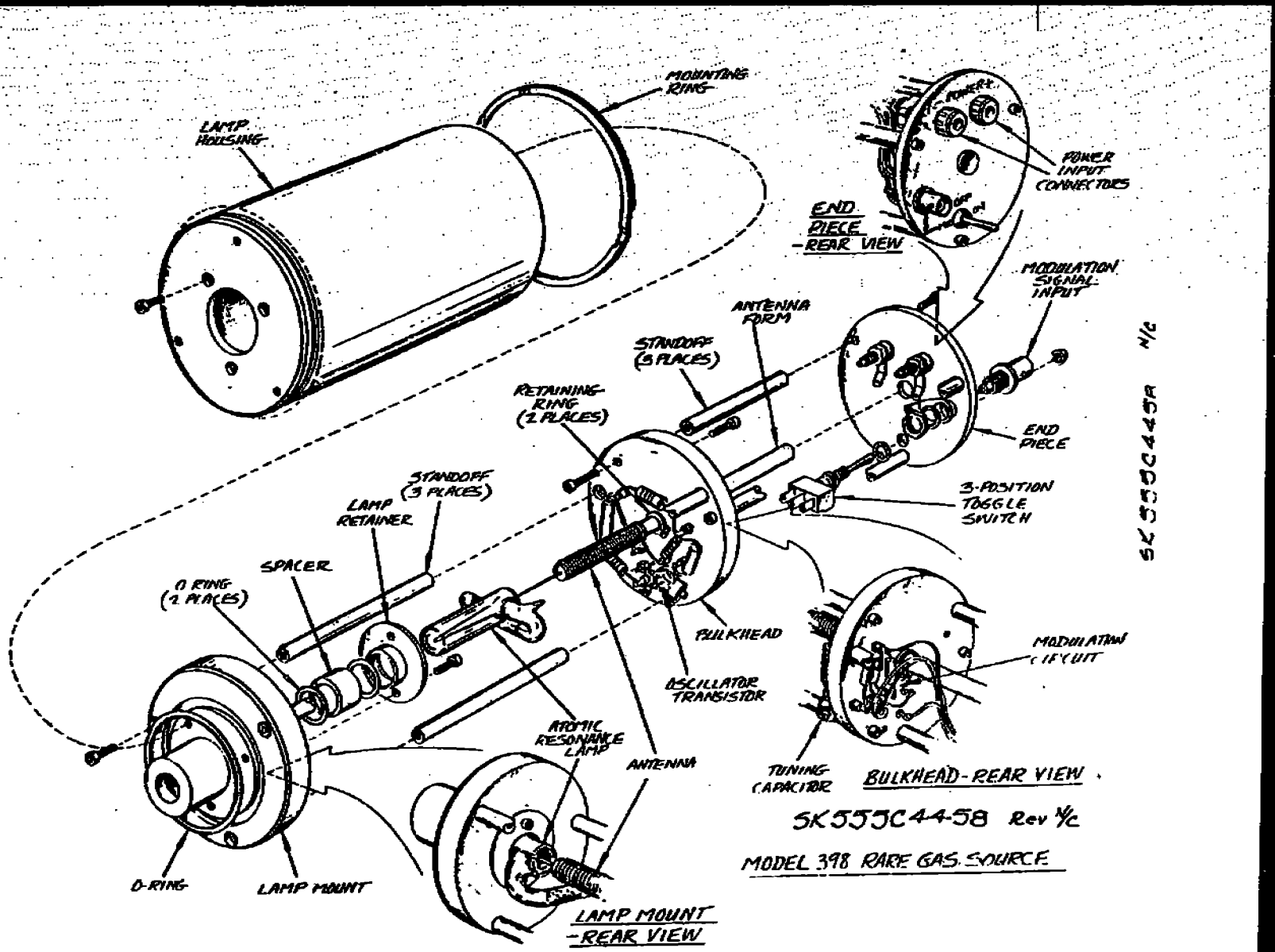

FIGURE B-7 QUANTATEC LAMP CONFIGURATION

CONTROL FUNCTIONS

Lamp:	On/Off or Modulated operation
Oscillator Voltage:	Variable from 20-35 volts
Source Heater:	Automatic Heater control for atomic sources

READOUT FUNCTIONS

±15V, 28V, VARIABLE OSCILLATOR VOLTAGE:**	Voltage readouts of power supplies
HTR PWR*:	Indicates power into source heater
TEMP*:	Actual temperature of source
TEMP SET*:	Setting temperature of source
INTENSITY*:	Intensity of visible light (arbitrary scale)
OSC LEVEL*:	Intensity of RF generator (arbitrary scale)
OSC AMPS*:	Oscillator current
BRD TEMP:	Circuit board temperature

*Indicates BNC connection at rear for recorders
**Available at rear for use with 385, 398 and 399 Exciters. The ±15 volts source can supply 1.2 amps, and the variable source can supply 1.5 amps.

POWER REQUIREMENT

115V, 60 Hz @ 1 ampere

DIMENSIONS

12" x 5" x 14"

LAMP POWER SUPPLY CONTROLLER UNIT MODEL 226-C

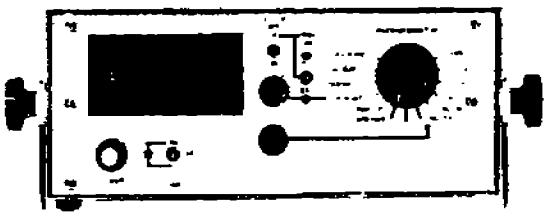

FIGURE B-8 QUANTATEC LAMP POWER SUPPLY

FIGURE 9 ATA CONTINUUM AND RADIANCE DISTRIBUTION

ALL DIM. IN INCHES

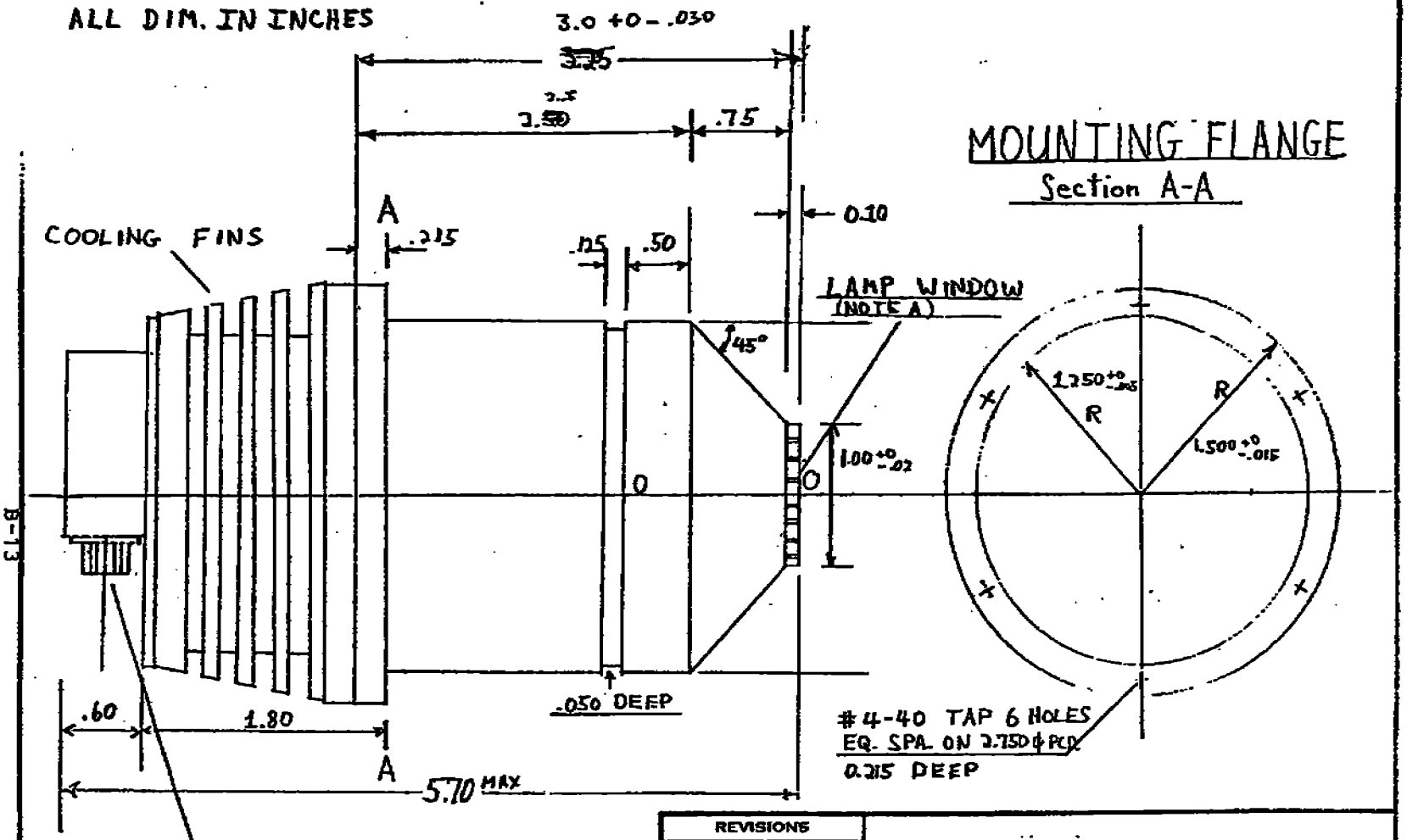

MOUNTING FLANGE

Section A-A

#4-40 TAP 6 HOLES
EQ. SPA. ON 2.750 ϕ PCD
0.215 DEEP

CONNECTOR CANNON DE-9P

NOTE A:

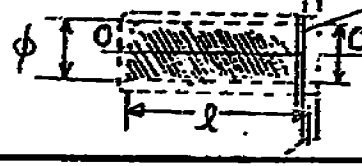

.240 CLEAR APERATURE
PLASMA IS
CYLINDRICAL WITH
DIM. 0.40ϕ x L10ℓ

REVISIONS			
NO.	DATE	BY	
1	31-10-81	WHM	
2			
3			
4			
5			

RESONANCE LTD.

LAMP HOUSING

DRAWN BY	SCALE	MATERIAL
WHM	1:1	
CHK'D	DATE	DRAWING NO
WHM	9-7-81	81A2-1
TRACED	APP'D	

APPENDIX C

NBS CALIBRATION REPORT FOR VSTOS

NATIONAL BUREAU OF STANDARDS

NATIONAL MEASUREMENT LABORATORY

CENTER FOR RADIATION RESEARCH

RADIOMETRIC CALIBRATION OF THE VSTOS

Contract No. RH4-117766

Martin Marietta Denver Aerospace

October, 1984

by

Jules Z. Klose

STATEMENT OF WORK

FAINT OBJECT SPECTROGRAPH (FOS)
VACUUM ST OPTICAL SIMULATOR (VSTOS)

RADIOMETRIC CALIBRATION

1. Objective: Perform absolute radiometric calibration of the FOS VSTOS from 120nm to 300nm.

2. Calibration: This calibration is a repeat of the VSTOS calibration completed in May 1984. The f/24 output of the VSTOS from each of the five lamps will be measured and compared with the known output of an Argon miniarc lamp.

3. Equipment: Martin Marietta Denver Aerospace (MMDA) will deliver the VSTOS, power supplies, test equipment and vacuum chamber and associated pumps to NBS and will return them to MMDA. NBS shall supply the vacuum monochromator and associated equipment and the standard lamp. NBS will provide support for unloading and loading the vacuum chamber at the receiving building and transportation between there and building 221.

4. Report: NBS shall reduce the data and provide an informal letter report.

5. Contacts: MMDA - Joe Vellinga (303) 977-3372
NBS Administrative - James Harmuth (301) 921-2707
NBS Technical - Dr. Jules Klose (301) 921-2356

Figures 1 and 2:

The data displayed in Figs. 1 and 2 was obtained using a mini-arc with an aperture of 0.015 in. The distance between the arc center and a 1 mm aperture mounted on the entrance slit of the NBS Seya-Namioka monochromator was 22.25 in.

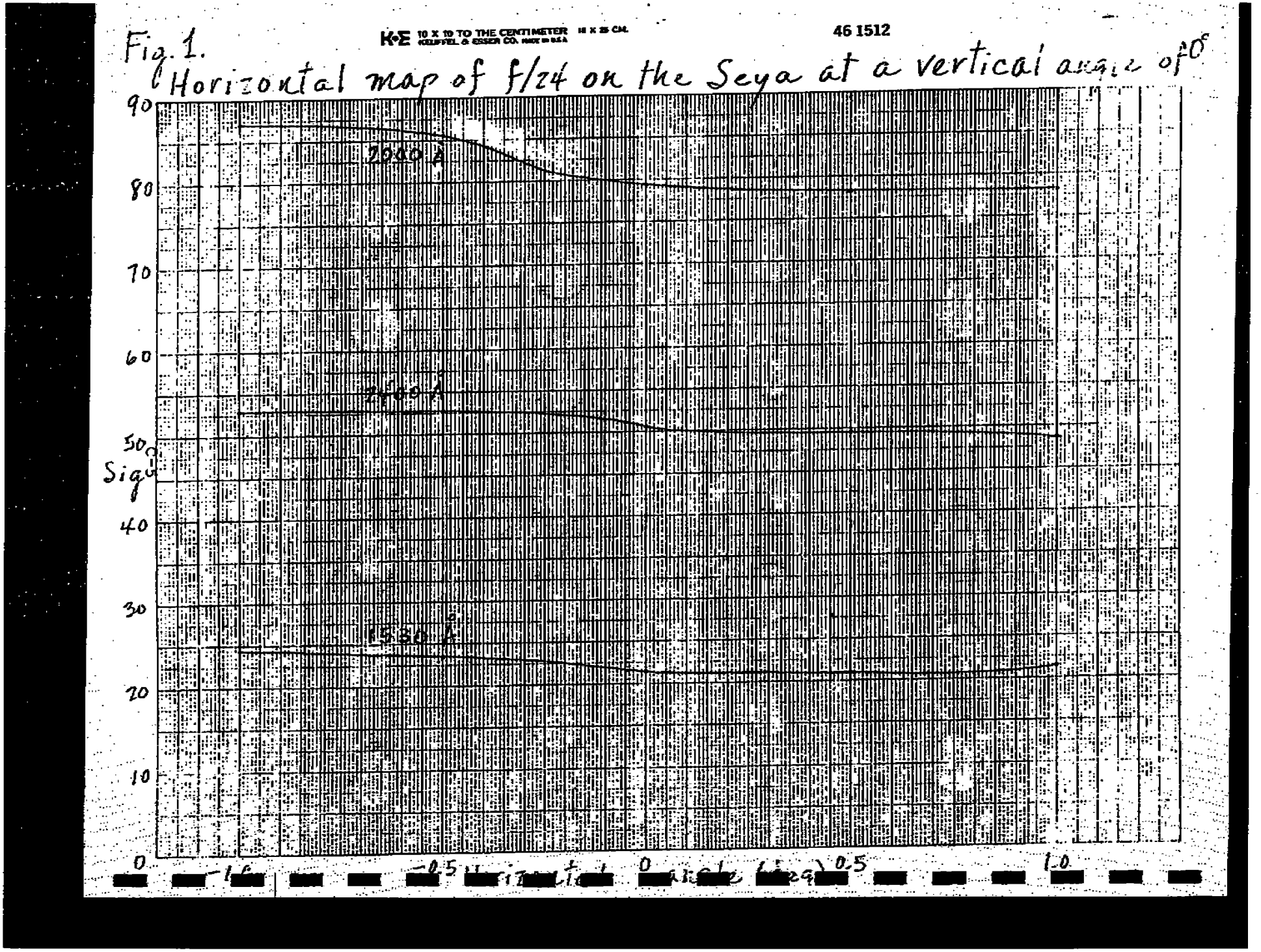
Fig. 1.
Horizontal map of f/24 on the Seya at a vertical angle of 0°
K+E 10 X 10 TO THE CENTIMETER
46 1512
90
80
70
60
50
40
30
20
10
0
2000 Å
2400 Å
1580 Å
Sigd
-1.0
-0.5
0
0.5
1.0

Fig. 2.

Vertical map of f/24 on the Seya at a horizontal angle of 0°.

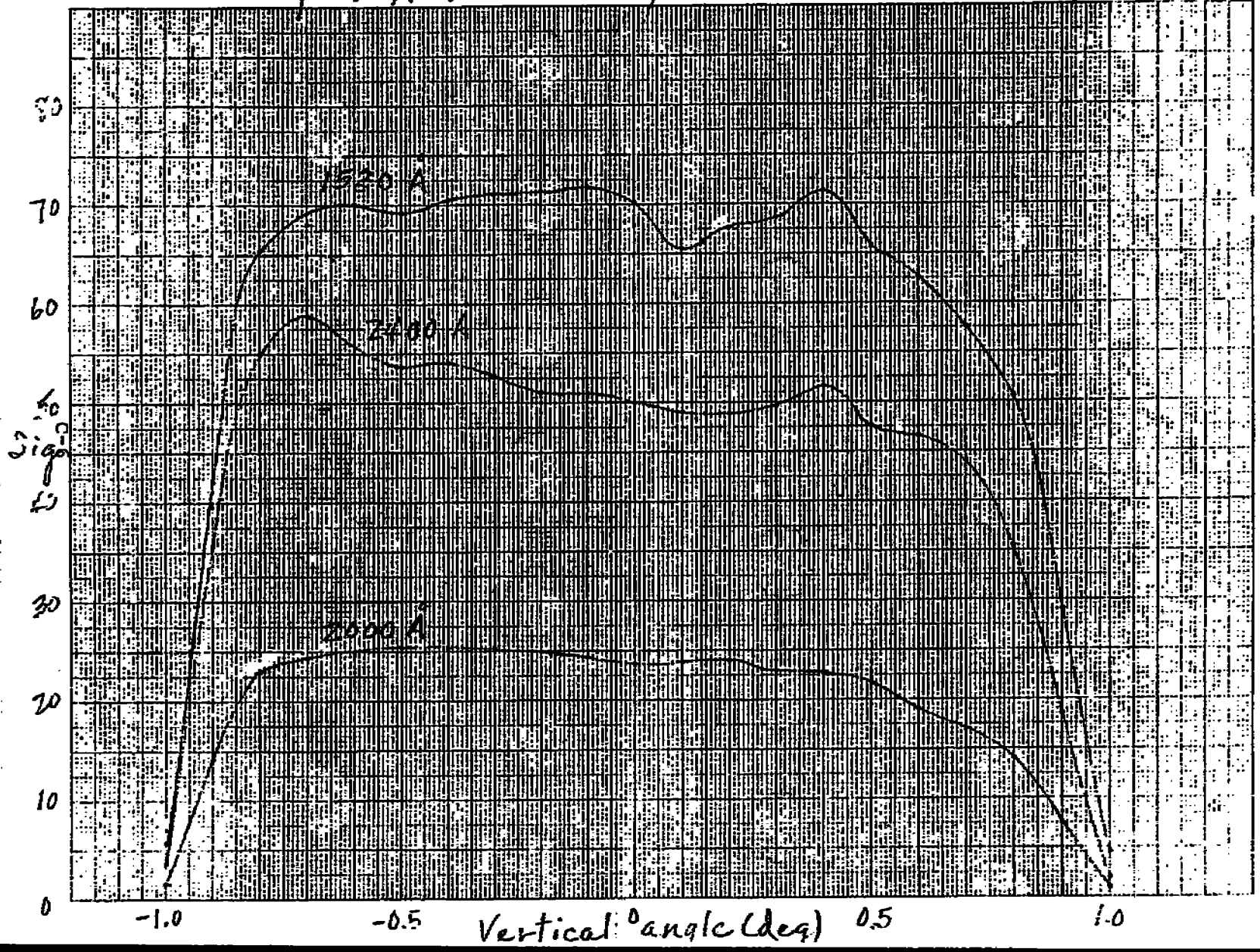

Figure 3:

The curve shown in Fig. 3 was obtained from map data such as that shown in Figs. 1 and 2 but for the entire range of wavelengths. The complete body of data was treated according to the map sample weights distribution over f/24 with a 0.37 central obscuration for the NBS Seya-Namioka monochromator.

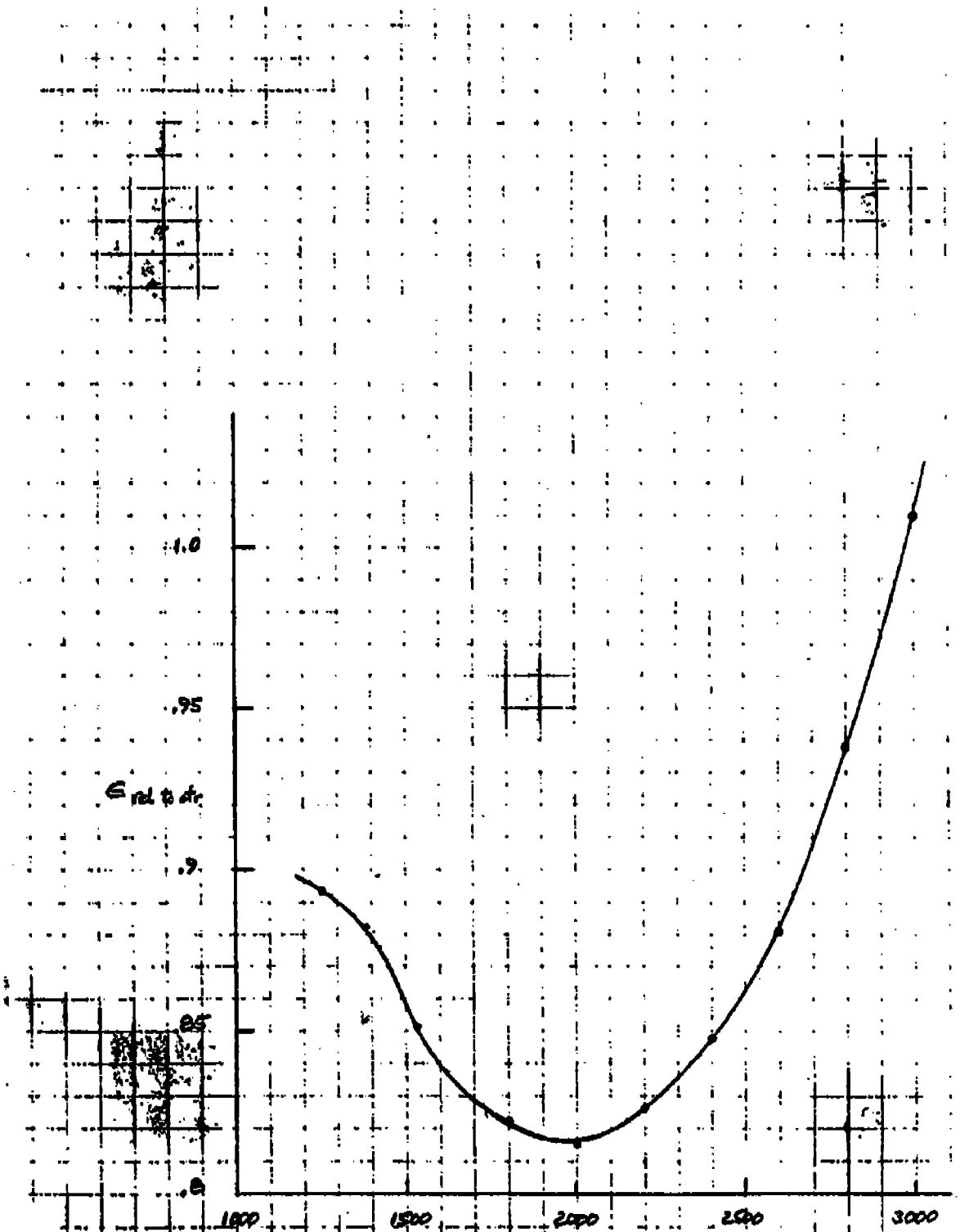

Fig. 3. Efficiency of ARBS Seya-Namioka Monochromator for VSTOS beam relative to center

Figures 4-8:

These figures give the spectral irradiances for the H_2, Ar, and Kr lamps in the VSTOS. These curves are plots of the post-FOS calibration data except as is noted for the Ar lamp. The measured values were corrected for the efficiency of the NBS monochromator over f/24 with a 0.37 central obscuration.

Fig. 4. Spectral irradiance of the H_2 lamps in the VSTOS.

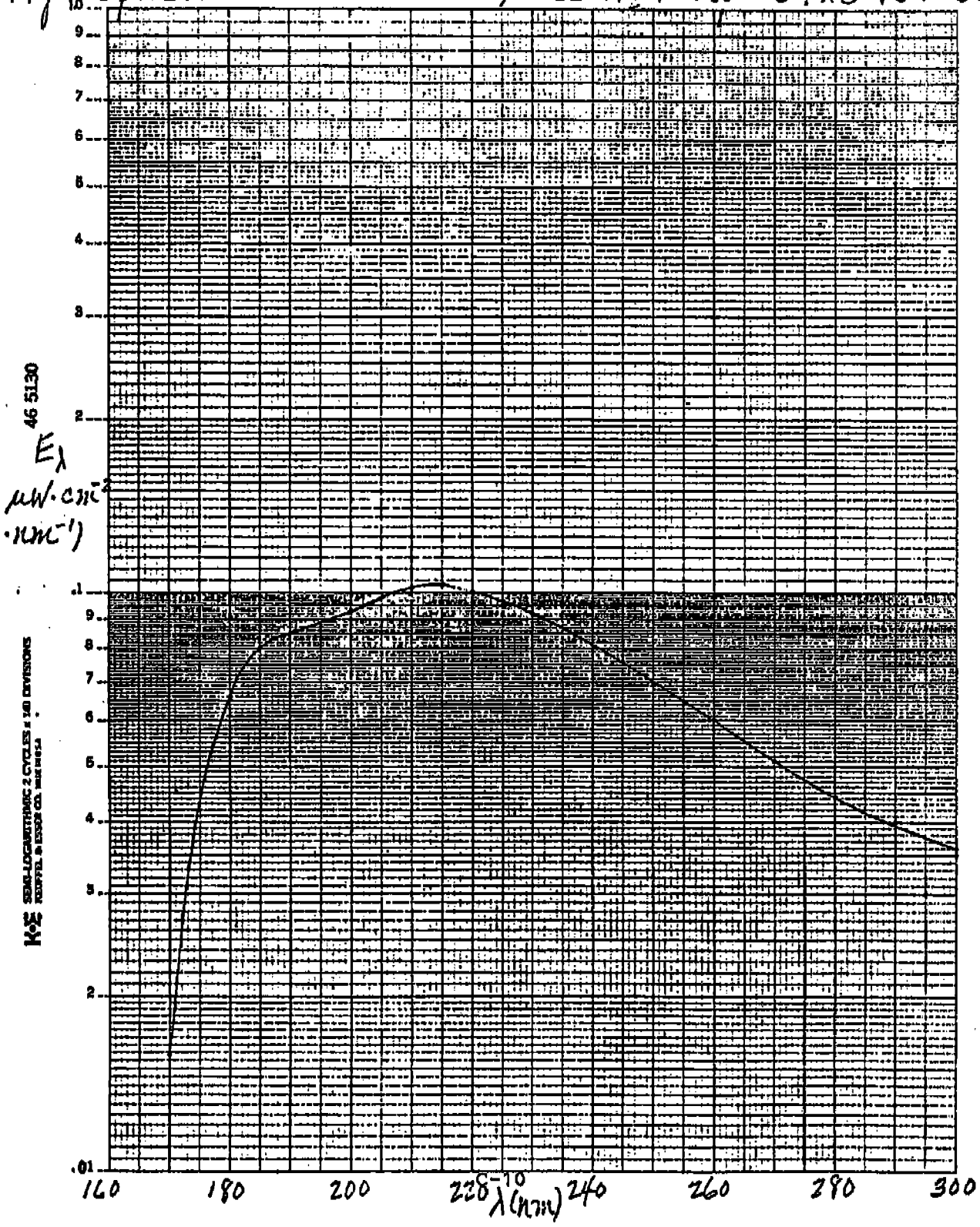

Fig. 5: Solar irradiance of the Irland in the VSTOS.

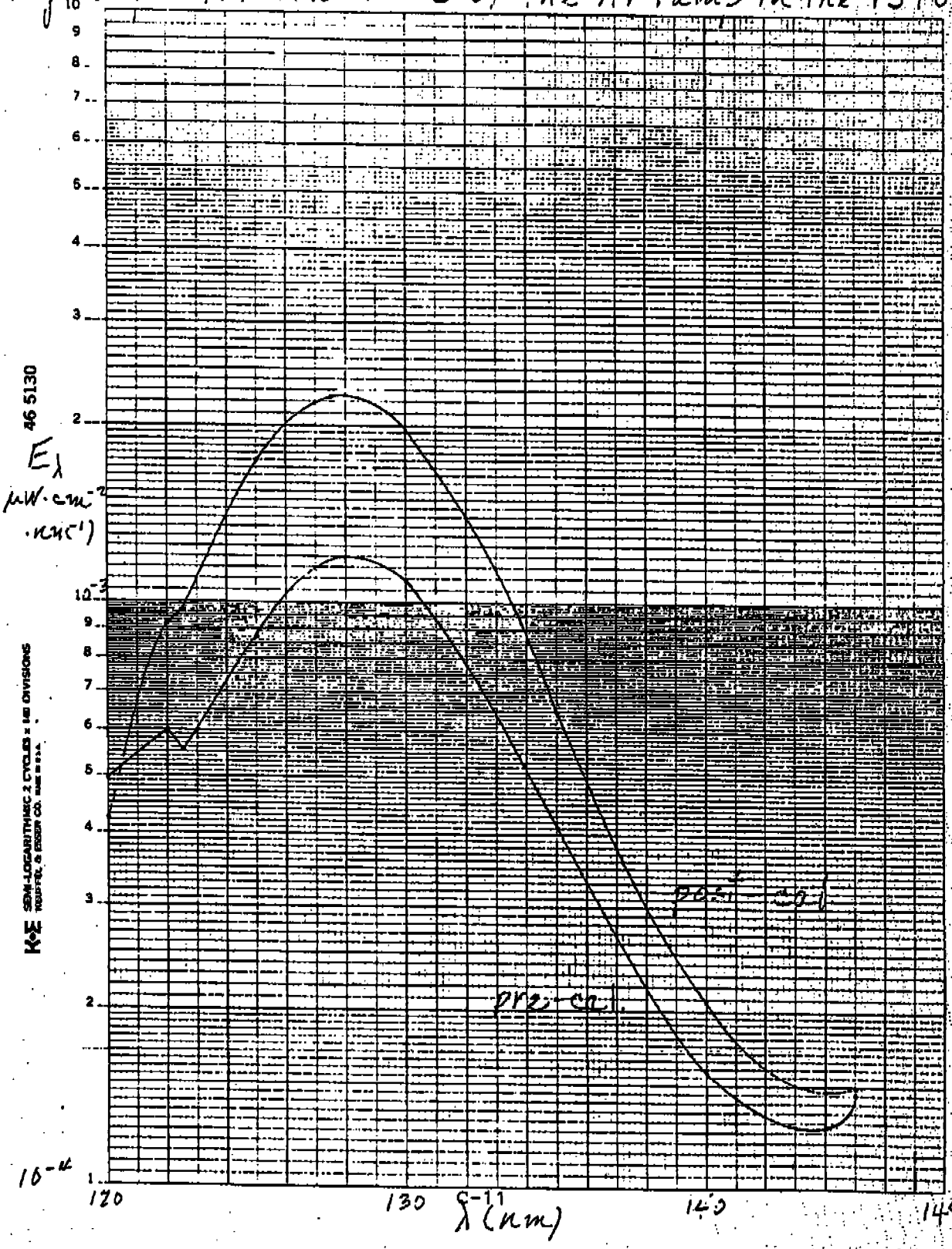

Fig. 6: Spectral irradiance of the Ar lamp in the VSTDS.

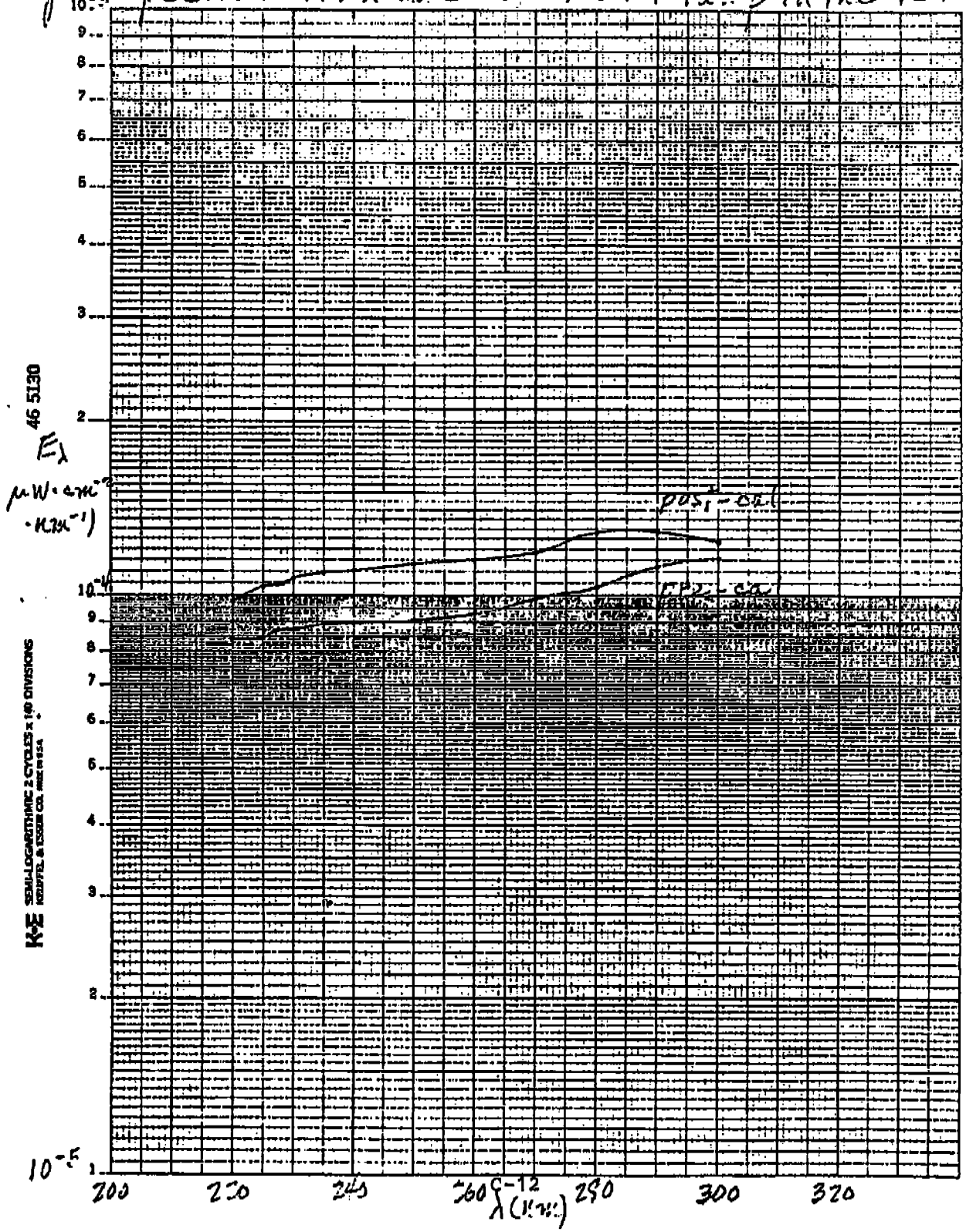

Fig. 7: Spectral irradiance of the Kr lamp in the VS-3

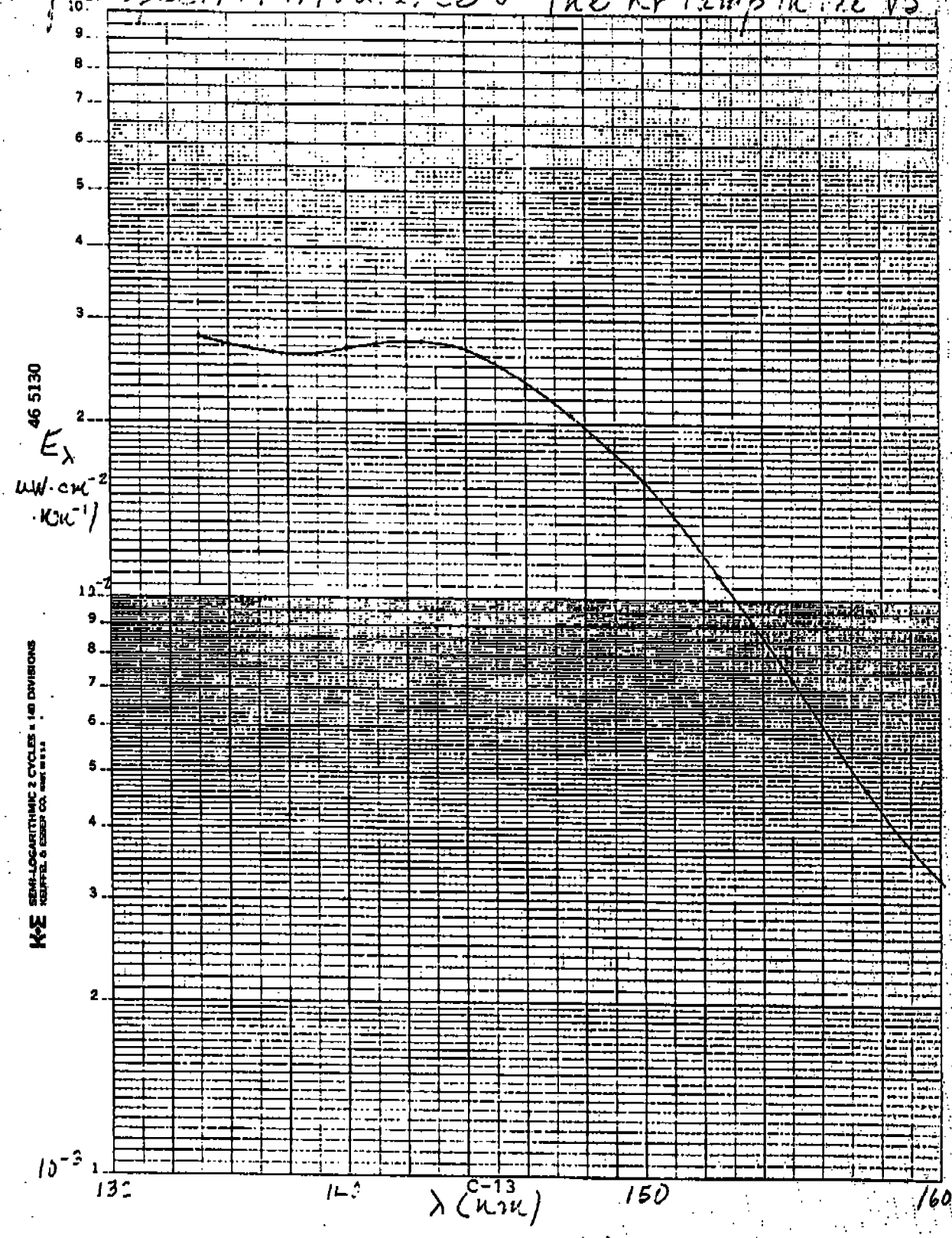

Fig. 8. Spectral irradiance of the Kr lamps in the VSTOS.

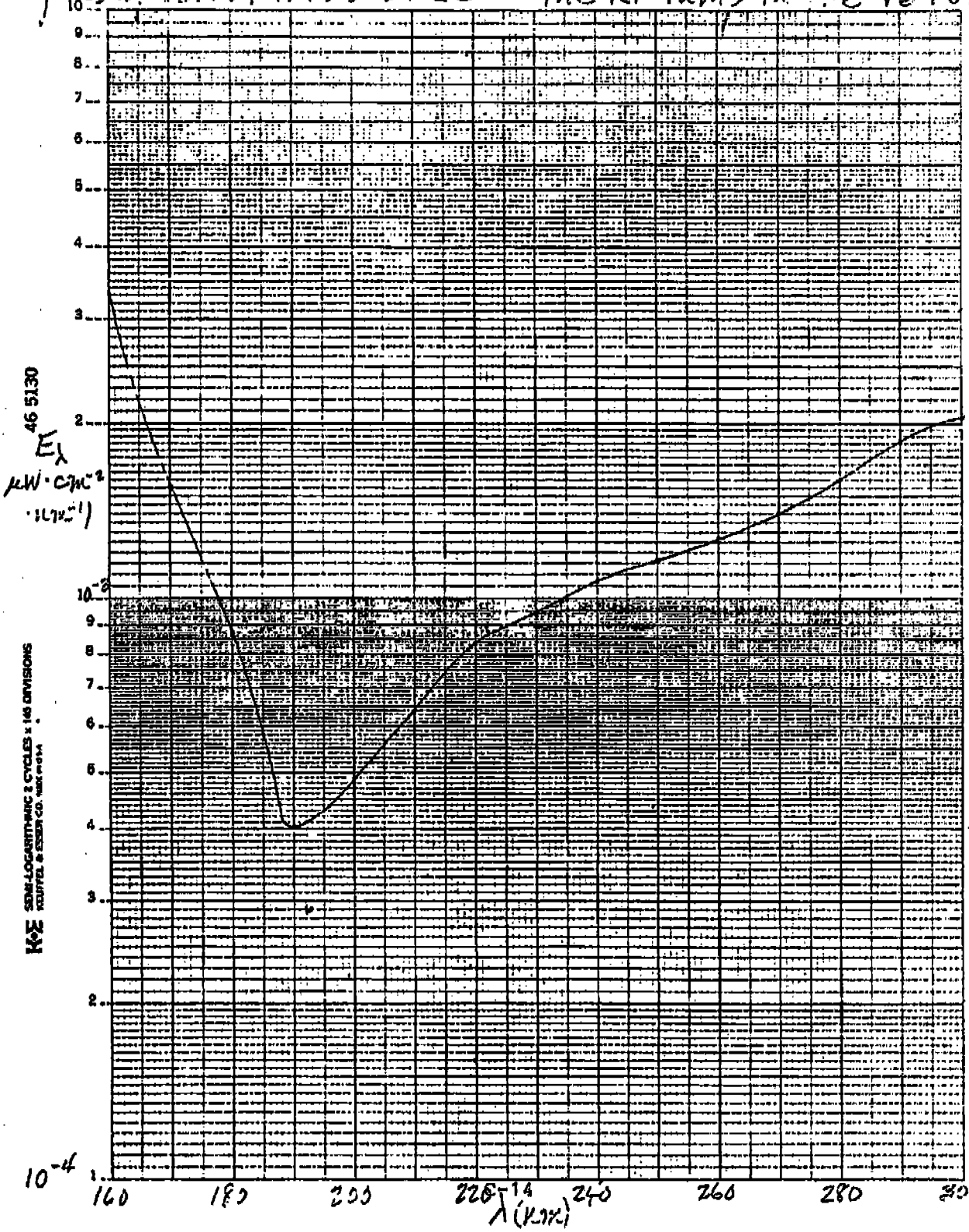

TABLE I. Line irradiances of Pt-Cr-Ne lamp 1 with a diffuser operated at 10 mA in the VSTOS prior to and subsequent to the calibration of the FOS.

λ(nm)	Species	E(μW . cm^{-2}) pre-FOS cal.	E (μW . cm^{-2}) post-FOS cal.
152.4725	Pt II	3.04 x 10^{-5}	2.73 x 10^{-5}
162.1658	Pt II	-	1.05 x 10^{-5}
166.8987	Pt II	-	1.06 x 10^{-5}
172.3128	Pt II	1.97 x 10^{-5}	2.03 x 10^{-5}
191.6083	Ne II	1.59 x 10^{-4}	1.26 x 10^{-4}
214.423, .424	Pt I, II	1.09 x 10^{-4}	9.29 x 10^{-5}
217.467	Pt I	8.54 x 10^{-5}	6.93 x 10^{-5}
226.2662	Pt II	3.42 x 10^{-5}	3.11 x 10^{-5}
235.7104	Pt I	-	2.27 x 10^{-5}
253.9200	Pt I	3.43 x 10^{-5}	3.25 x 10^{-5}
262.8031	Pt I	1.07 x 10^{-4}	9.96 x 10^{-5}
273.3961	Pt I	1.55 x 10^{-4}	1.38 x 10^{-4}
292.9795	Pt I	1.68 x 10^{-4}	1.55 x 10^{-4}

TABLE II. Line irradiances of Pt-Cr-Ne lamp 2 operated at 10 mA in the VSTOS prior to and subsequent to the calibration of the FOS.

λ(nm)	Species	E(μW . cm^{-2}) pre-FOS cal.	E (μW . cm^{-2}) post-FOS cal.
124.8600	Pt II	.00158	.00116
140.3896	Pt II	.00261	.00180
152.4725	Pt II	.00730	.00529
162.1658	Pt II	.00111	.000918
166.8987	Pt II	.00201	.00148
172.3128	Pt II	.00215	.00174
191.6083	Ne II	.0172	.0116
214.423, .424	Pt I, II	.0113	.00838
217.467	Pt I	.00863	.00701
226.2662	Pt II	.00386	.00297
235.7104	Pt I	.00297	.00227
253.9200	Pt I	.00333	.00261
262.8031	Pt I	.0116	.00910
273.3961	Pt I	.0145	.0124
292.9795	Pt I	.0183	.0150

TABLE III. Spectral irradiance of the hydrogen lamp operated in the VSTOS at an oscillator setting of 28 volts prior to and subsequent to the calibration of the FOS.

λ(nm)	E_λ(μW . cm^{-2} . nm^{-1}) pre-FOS cal.	E_λ(μW . cm^{-2} . nm^{-1}) post-FOS cal.
170.0	.0193	.0158
180.0	.0720	.0652
185.0	-	.0800
190.0	.0935	.0847
200.0	.100	.0928
210.0	.105	.102
215.0	-	.103
220.0	.101	.100
230.0	.0891	.0916
240.0	.0768	.0801
250.0	.0665	.0693
260.0	.0572	.0598
270.0	.0496	.0511
280.0	.0430	.0442
290.0	.0381	.0396
300.0	.0347	.0351

TABLE IVa. Spectral irradiance of the Ar dimer lamp operated in the VSTOS at a power level of 6.13 W prior to and subsequent to the calibration of the FOS.

λ(nm)	E_λ(μW . cm^{-2} . nm^{-1}) pre-FOS cal.	E_λ(μW . cm^{-2} . nm^{-1}) post-FOS cal.
120.0	.000494	.000422
122.0	.000600	.000913
122.5	.000553	.000970
125.0	.000869	.00174
127.5	-	.00224
130.0	.00109	.00197
135.0	.000411	.000645
140.0	.000157	.000208
144.0	.000128	.000147
145.0	.000145	.000149

TABLE IVb. Spectral irradiance of the Ar dimer lamp operated in the VSTOS at a power level of 6.13 W prior to and subsequent to the calibration of the FOS.

λ(nm)	E_λ(μW . cm^{-2} . nm^{-1}) pre-FOS cal.	E_λ(μW . cm^{-2} . nm^{-1}) post-FOS cal.
220.0	8.39×10^{-5}	9.76×10^{-5}
225.0	8.44×10^{-5}	1.03×10^{-4}
227.5	8.68×10^{-5}	1.04×10^{-4}
230.0	8.72×10^{-5}	1.07×10^{-4}
235.0	8.91×10^{-5}	1.09×10^{-4}
240.0	8.95×10^{-5}	1.10×10^{-4}
250.0	9.07×10^{-5}	1.13×10^{-4}
260.0	9.30×10^{-5}	1.15×10^{-4}
270.0	9.86×10^{-5}	1.18×10^{-4}
280.0	1.03×10^{-4}	1.28×10^{-4}
290.0	1.12×10^{-4}	1.28×10^{-4}
300.0	1.16×10^{-4}	1.23×10^{-4}